NASA-CR-121186

WANL-FR-NAS3-16819-8

FINAL REPORT

ANALYSIS OF TEMPERATURE AND PRESSURE DISTRIBUTION OF CONTAINERS FOR NUCLEAR WASTE MATERIAL DISPOSAL IN SPACE

BY

L. E. VAN BIBBER AND W. G. PARKER

ASTRONUCLEAR LABORATORY
WESTINGHOUSE ELECTRIC CORPORATION

PREPARED FOR
NATIONAL AERONAUTICS AND SPACE ADMINISTRATION

NASA LEWIS RESEARCH CENTER

CONTRACT NAS 3-16819

Requests for copies of this report should be referred to

National Aeronautics and Space Administration
Scientific and Technical Information Facility
P.O. Box 33
College Park, Md. 20740

1. Report No.	2. Government Accession No.	3. Recipient's Catalog No.
NASA-CR-121186		

4. Title and Subtitle	5. Report Date
FINAL REPORT - ANALYSIS OF TEMPERATURE AND PRESSURE DISTRIBUTION OF CONTAINERS FOR NUCLEAR WASTE MATERIAL DISPOSAL IN SPACE	April 1973
	6. Performing Organization Code
7. Author(s)	8. Performing Organization Report No.
L. E. VanBibber and W. G. Parker	WANL-FR-NAS3-16819-8
	10. Work Unit No.
9. Performing Organization Name and Address Westinghouse Electric Corporation Astronuclear Laboratory P. O. Box 10864 - Pittsburgh, Pa. 15236	11. Contract or Grant No. NAS 3-16819
	13. Type of Report and Period Covered Contractor Report
12. Sponsoring Agency Name and Address National Aeronautics & Space Administration Washington, D.C. 20546	14. Sponsoring Agency Code

15. Supplementary Notes
Project Manager, Richard Puthoff, Power Systems Division,
NASA Lewis Research Center, Cleveland, Ohio

16. Abstract

A computer program (ESATA) was adapted from a previous generation program to analyze the temperature and internal pressure response of a radioactive nuclear waste material disposal container following impact on the earth. This program considers (in addition to the standard modes of heat transfer) component melting, LiH dissociation, temperature dependent properties and pressure and container stress response. Analyses were performed for 21 cases with variations in radioactive power level, container geometry, degree of deformation of the container, degree of burial and soil properties. Results indicated that the integrity of SS-316 containers could be maintained with partial burials of either undeformed or deformed containers. Results indicated that completely buried waste containers, with power levels above 5 KW, experienced creep stress rupture failures in 4 to 12 days.

17. Key Words (Suggested by Author(s))	18. Distribution Statement
Nuclear Waste Disposal Nuclear Safety Soil Burial	Unclassified - Unlimited

19. Security Classif. (of this report)	20. Security Classif. (of this page)	21. No. of Pages	22. Price*
Unclassified	Unclassified	111	$3.00

* For sale by the National Technical Information Service, Springfield, Virginia 22151

Page Intentionally Left Blank

FOREWORD

This is the final report for the project entitled "Analysis of Temperature and Pressure Distribution of Containers for Nuclear Waste Material Disposal in Space." The work was performed under NASA Contract NAS 3-16819.

The Program Manager for Westinghouse was Mr. A. R. Jones. The contributors to this study included Messrs. W. G. Parker, L. E. VanBibber and B. S. Preble.

Page Intentionally Left Bl

TABLE OF CONTENTS

TABLE OF CONTENTS (Continued)

TABLE OF CONTENTS (Continued)

LIST OF ILLUSTRATIONS

LIST OF TABLES

SUMMARY

A multi-dimensional transient heat transfer analysis computer program (ESATA - Executive Subroutines for Afterheat Temperature Analysis) was adapted to analyze the temperature and pressure response of a radioactive nuclear waste disposal container following impact on the earth. The ESATA program consides (in addition to standard modes of heat transfer) component melting, LiH dissociation, the transport property variation, pressure response and container creep stress buildup. This program was tailored to analyze both undeformed and deformed waste disposal containers with varying degrees of ground burial from zero to deep burial with minimum input requirements.

For this study, a general waste disposal container design was considered consisting of concentric spherical layers of nuclear wastes, tungsten shielding, LiH shielding and SS-316 container. twenty-one cases were analyzed for post impact periods of up to 23 days. Variations were considered in the nuclear waste material power level ranging from 1.5 to 30 KW, radii of materials, degree of deformation, degree of burial and soil properties. Power levels were assumed constant during the transient and the initial internal pressure of 25 psi was based on helium release from α emitters. Initial temperatures reflected the heat generation during reentry. No provision was made in the analysis for methods of relieving internal pressures. Typical results of these analyses included:

- The integrity of the waste containers was maintained for the partial burial (up to 38% diametral) of both undeformed and deformed containers during the transient.
- Complete burial of waste containers with more than 5 KW of radioactive waste material resulted in creep stress rupture failures occurring 4-12 days after impact.
- At time of rupture, container temperatures were in the range of 2500-2600^{o}R and the internal pressure was approximately 130 psi.

- Hydrogen release from LiH dissociation was the primary cause of the pressure response.
- Temperature response of the container was sensitive to soil properties but not depth of burial, other than partial burial.

1.0 INTRODUCTION

With an increasing number of nuclear power plants going into service, the problem of disposal of the radioactive waste, obtained from the reprocessing of the spent fuel elements, becomes significant. The U. S. Atomic Energy Commission currently has the responsibility of safe handling of this nuclear waste. Their basic requirement[1] is to either store or dispose the waste in such a manner that it will neither endanger those people closely involved nor the general public. Furthermore, it must be managed in such a way that it will not have an adverse impact on man's environment.

The AEC has considered several concepts for the disposal or storage of the radioactive nuclear waste. One of these concepts is to dispose the waste into space. The National Aeronautics and Space Administration has been assigned the task of determining the feasibility of such a method. In this feasibility study, many areas of safety must be studied and evaluated. One of these areas involves the safety of the package on an aborted flight or trajectory resulting in the package returning and impacting on the earth. At impact, the package must withstand the impact forces and contain the radioactive waste material. After impact, the heat due to the decaying waste material must be dissipated to prevent the container from failing. This requirement becomes difficult when the package either partially or completely buries itself in the ground. Therefore, for this portion of the safety analysis, Westinghouse Electric Corporation, Astronuclear Laboratory, under contract NAS3-16819, has provided analytical assistance to NASA - Lewis Research Center.

The analysis of the system subsequent to impact is quite complex. In addition to the standard modes of heat transfer, conduction, convection and radiation, other phenomena must be considered in the analysis. Melting of the fuel, shielding containment system and soil may occur; therefore, the heat of fusion of these components must be included in the analysis. If a shielding material such as LiH is used, dissociation must also be considered. The containment system will have an initial internal pressure which will increase during the transient due to heating of helium released from α emitters and due to the dissociation of hydride materials. The containment vessel will, therefore, be subjected to both heating and pressure loading. The creep rupture characteristics of the material selected for the containment vessel must be evaluated in assessing the survival probability of the system.

The complexity of the analysis of the post impacted system is further compounded by the consideration of variable soil conditions, burial depths and deformation of the waste and containment system. Since the analysis of the post impact event is not straightforward and is difficult to describe by simple analytical models, a computer program developed for the post impact analysis of a reactor/containment system was used. This program called Executive Subroutines for the Afterheat Temperature Analysis (ESATA) was developed by Westinghouse under a NASA contract NAS3-14405[2] and an Air Force Contract F29601-72-C-0035[3] to analyze the transient afterheat temperatures and pressure response of a reactor/containment system following impact. This program is a multi-dimensional transient heat transfer analysis program that was expanded to include such phenomena that is pertinent to this program such as the following:

- System component melting
- Melting of the soil which surrounds the system
- LiH dissociation
- Internal pressure buildup due to LiH dissociation and presence of helium
- Containment vessel creep rupture analysis

The program was also changed to provide:

- Internally generated models of deformed and undeformed containment system configurations
- Variable degree of soil burial

The objectives of this study were to adapt the ESATA code to evaluate the waste disposal containment system during the post impact period and to perform heat transfer calculations of various waste container designs under varying impact conditions. A three task program was implemented to accomplish the study objectives which include:

- Task I - Adaption of the ESATA Code
- Task II - Heat Transfer Calculations
- Task III - Reporting

Task I consisted of adapting the ESATA computer program to evaluate nuclear waste container designs. This effort included the modification of the internally stored nodal models to better represent the containment system and to expand the capability of analyzing variable soil burial conditions. A description of the ESATA program with adaptions is presented in Section 2. For Task II, 21 cases were analyzed under transient post impact conditions. These cases considered variations in decay energy level, waste material composition, waste and containment system dimensions, degree of deformation, degree of burial and soil properties. Section 3 describes the results of these calculations. Conclusions obtained from this study are presented in Section 3. Operating instructions for using the ESATA code are presented in Appendix A. Appendices B and C contain the property data used for these analyses and symbols used in the computer code.

2.0 TASK I. - ADAPTION OF THE ESATA CODE

The ESATA program was modified to analyze the thermal safety aspects of post-impacted radioactive nuclear waste containment systems. Specifically, the program calculates the transient temperature and pressure response of a containment system (Figure 2-1) after impact. The analysis considers a system containing helium released from α emitters and radioactive decay energy. The decay heat must be dissipated by conduction through the containment material to the environment. The pressure from the helium and hydrogen generation must be contained while the heat is being dissipated.

The main components of these systems include:

- Waste Material Composite of:
  - Lithium Hydride
  - Aluminum
  - Copper
  - Spent Fuel
- Inner Shell (Tungsten)
- Shielding (LiH)
- Outer Container (SS-316)

The following phenomena are simulated in the analysis:

- Melting of each constituent in the composite waste material.
- Melting of containment material, shielding and soil.
- Lithium hydride dissociation.
- Pressure buildup inside the containment vessel due to increased temperatures of the helium released from α emitters and hydrogen released from hydride dissociation.
- Creep rupture analysis of the containment vessel.

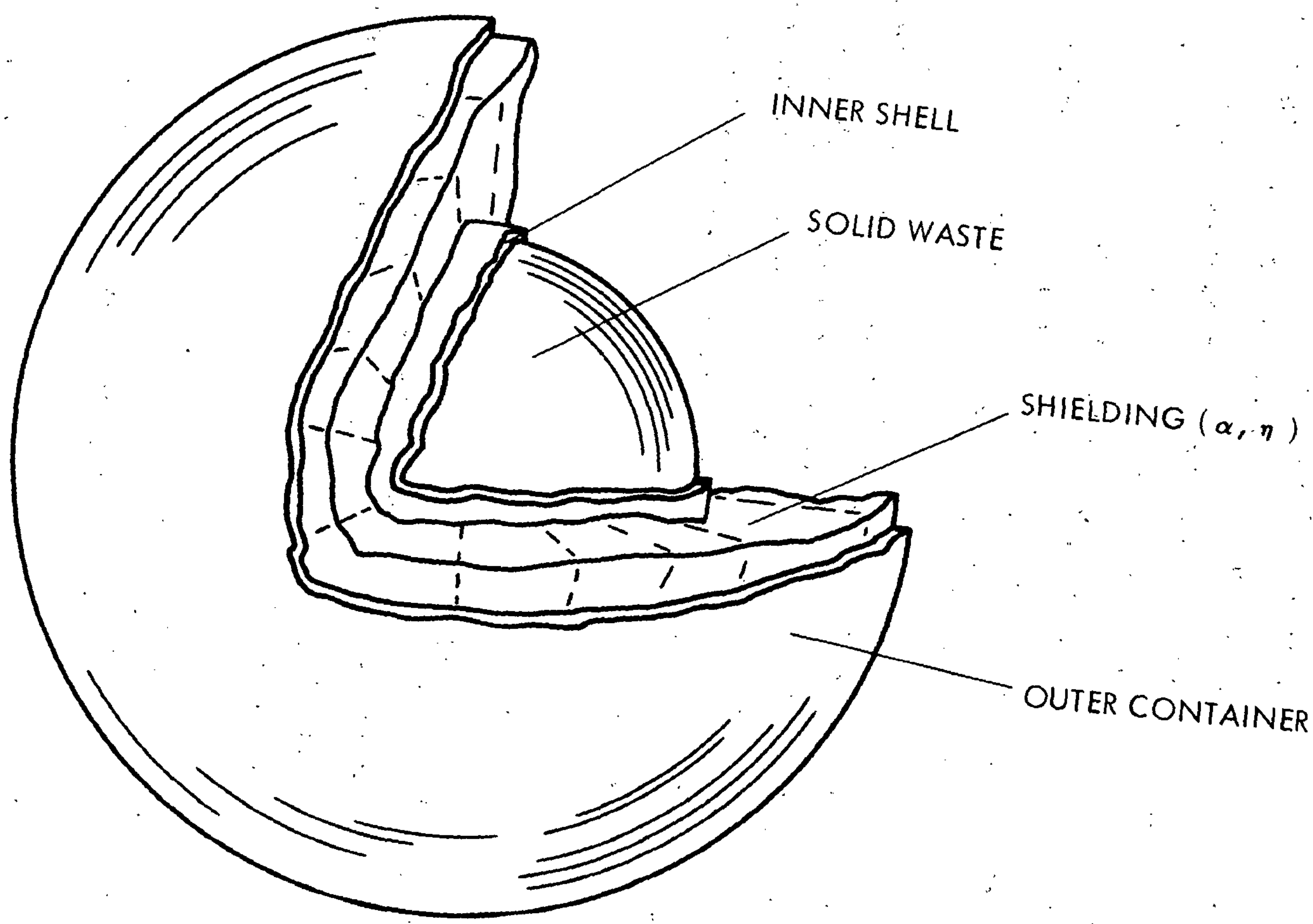

Figure 2-1. Radioactive Nuclear Waste Container Configuration

The program was originally developed to analyze mobile nuclear power plants. For this study, the internally developed nodal models were modified to provide for simulation of spherical waste containment systems with or without deformation. Flexibility was built into the program to consider variable constituent weights and power levels for the waste material. Flexibility was provided for variable dimensions, temperatures and materials for the waste container and environment. The treatment of burial conditions was expanded to consider variable soil-to-vessel interface conditions and to consider variable burial positions from "zero" to fully buried conditions for the undeformed and deformed configurations. Furthermore, the undeformed configuration could be analyzed for varying depths below the surface of the soil.

This program was originally developed using the TAP-A[4] computer program as a nucleus. The TAP-A computer program, developed by Westinghouse, solves problems involving transient and steady-state heat transfer in multi-dimensional systems having arbitrary geometric configurations, boundary conditions, initial conditions and physical properties. The capabilities of TAP-A have been maintained in the ESATA program.

2.1 PROGRAM DESCRIPTION

2.1.1 General Description of Code

Figure 2-2 presents a schematic flow chart of the ESATA code package. Each of the subroutines contained in the ESATA code are identified in the figure including the general sequence in which they are executed by the program.

2.1.2 Calculational Procedure of Code

Step 1 Input data is read by the main program routine ESATA and by subroutines INPUTT and HTMGEN.

Step 2 The input data are processed and nodal structure representations for the waste container are set up in subroutine HTMGEN.

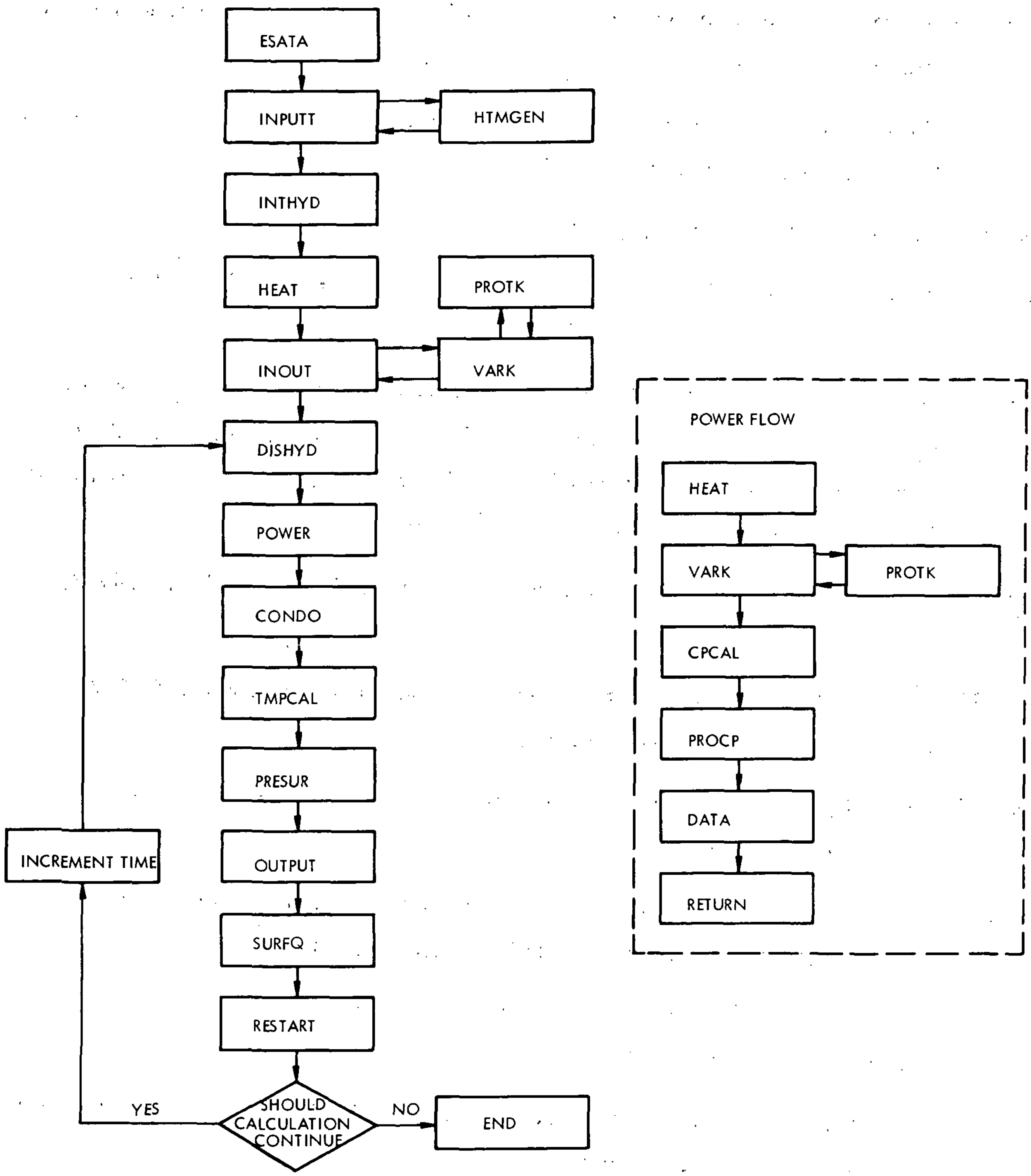

Figure 2-2. ESATA Code Package Schematic Flow Chart

Step 3 Parameters are initialized in INTHYD for the simulation of hydride dissociation.

Step 4 The total heat generation rate is distributed among those nodes representing heat sources in subroutine HEAT.

Step 5 The input data, the geometry setup, the initial heating rate distribution, and initial temperatures are output by subroutine INOUT.

Step 6 Time is incremented by a predefined amount.

Step 7 Heat source distributions due to hydride dissociation are established for the time interval in DISHYD.

Step 8 Temperature dependent material properties (such as thermal conductances and capacitance) to be held constant during the time interval are established by subroutine POWER. Note that subroutine POWER calls subroutines as indicated in Figure 2-2 during the process of establishing these data.

Step 9 Temperatures for all system components are computed in subroutines CONDO and STCALC.

Step 10 Melting of all component represented are established in subroutine TMPCAL based on the computed temperatures.

Step 11 Internal pressure buildup and the corresponding containment vessel stress level is computed in subroutine PRESUR.

Step 12 Temperature distributions, pressure, heat source distributions and the fraction of melting of each component is printed by subroutine OUTPUT.

Step 13 All common block data is stored on an auxiliary tape at predefined intervals for restart capability in RESTART.

Step 14 Time is again incremented and steps 7-13 repeated. The calculation is terminated when the run time is exceeded.

2.1.3 Internal Node Generators

Three generalized heat transfer models (HTM's) of post impacted nuclear waste containment systems were developed and stored in the ESATA program to minimize input data requirements. These models represent the undeformed configuration in a partial burial, the deformed configuration in a partial burial, and the undeformed configuration in a shallow-to-deep burial.

Undeformed HTM

The undeformed HTM for partial burial analysis is shown in Figure 2-3. This model contains 12 internal nodes. A total of 14 layers with 8 nodes in each layer are available to simulate the waste container and environment. Basic modeling assumptions for this configuration are:

- Two-dimensional analysis
- No internal deformation with structure intact.

Representation of the containment system are limited to the first 12 layers with a layer required to represent the interface conditions between the container and the environment and at least one layer required to represent the soil and/or air. The radii, material representation and initial temperatures can be varied for each layer via input. Earth burial from zero to 100% can be considered through the input of nodes (0-8) circumferentially in a layer that represents the environment external to the containment vessel.

The waste product material can be represented for all three models as a composite of the following four components by the selection of material number 49 to represent the heat sources (see Appendix B):

Lithium-Hydride
Aluminum
Copper
Spent Fuel

Weights of each component is specified via input. Density and specific heats are calculated for the waste material based on the component weights. A fixed thermal conductivity of 17 Btu/Hr-Ft-$^{\circ}$F is used, and the melting of each component in the waste material is simulated.

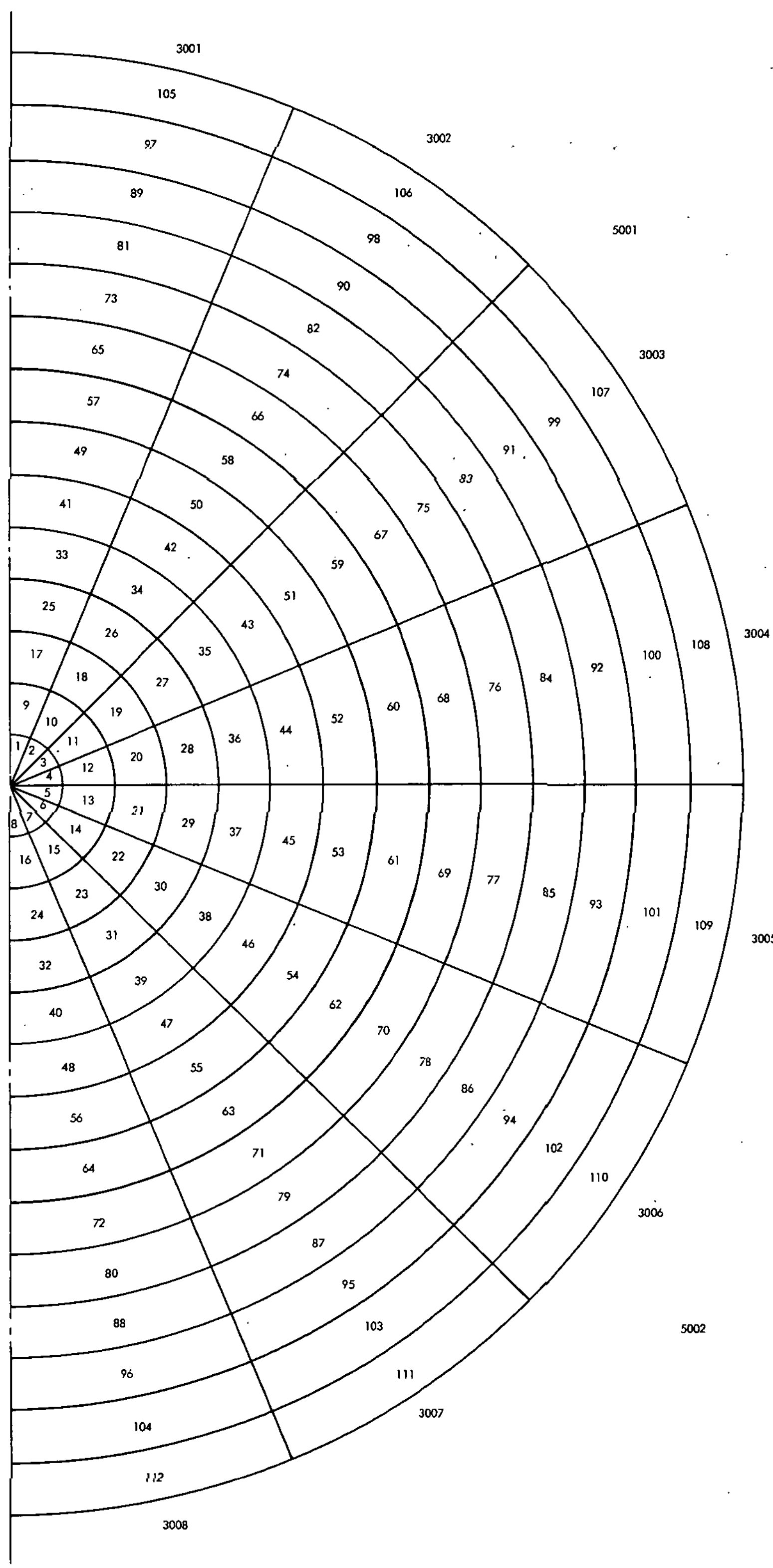

Figure 2-3. HTM-1 Undeformed Model

Deformed HTM

Figure 2-4 describes the nodal model for representing the waste container in a deformed configuration. This model contains 252 internal nodes. Modeling assumptions applicable to the deformed model include:

- Two-dimensional analysis.
- Deformation of waste material, shielding and containment in lower half of system only.
- Degree of deformation is variable via input of node layer thicknesses for the deformed region.

Consistent with the undeformed model, 14 layers of nodes are provided in the spherical undeformed region with 4 nodes in each layer. In the cylindrical region representing the deformed base, there are also 14 layers with 14 nodes in each layer. With this pattern, each layer in the undeformed section is modeled discretely in the deformed section. For example, the third layer in the undeformed section is represented by nodes 37 to 40. Nodes representing the third layer in the deformed section would include nodes 41-43, plus nodes 7 and 25. Consistent with the undeformed model, the temperatures, radii and material selection for the undeformed sections are specified in the input. Nodes representing this layer in the deformed section are also assigned the same material and temperature. The spherical radii in the undeformed section are identical to the cylindrical radii in the deformed section. For the deformed model, an additional input of thicknesses of each row of nodes is required. These thicknesses are applied to all 14 nodes in each row (for example, nodes 5, 23, 41, ---, 221, 239 all assigned one thickness). The number of layers available for representing the waste containment system is limited to 12 similar to the undeformed model. The degree of burial can be varied from zero to 100%. For zero burial, all nodes in rows below the containment vessel represent soil. Partial burials are defined by inputting the number of nodes in each layer that represent air. For the deformed model, this number can be varied from 0 up to a number equal to the sum of number of layers representing the waste containment system + 4. (This defines all nodes on the side of the containment vessel as being exposed to air.)

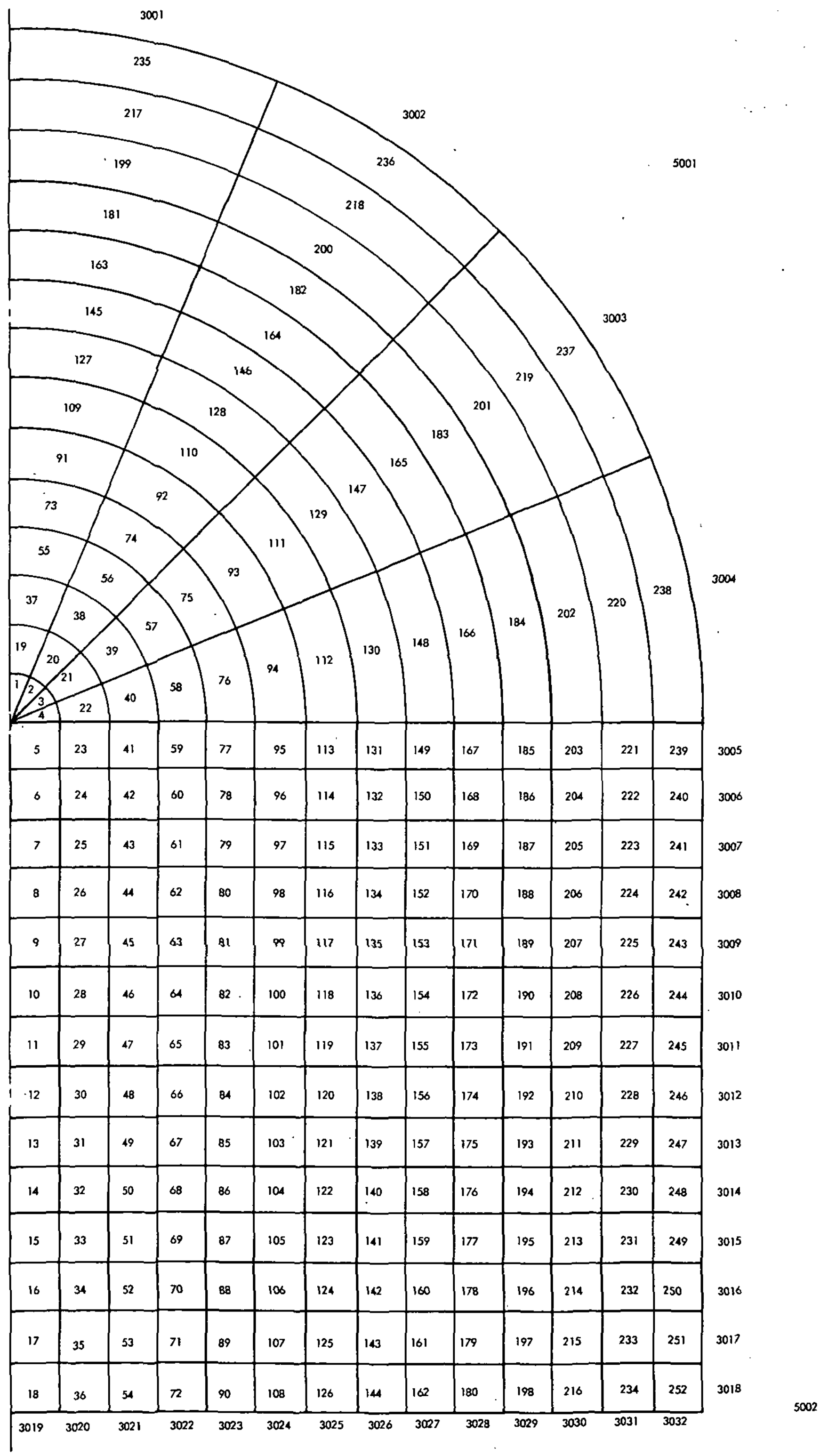

Figure 2-4. HTM-2 - Deformed Model

Undeformed HTM - Deep Burial

The third nodal model, shown in Figure 2-5, represents the undeformed model in varying degrees of deep burial. This model is represented by 270 nodes. Basic modeling assumptions are identical to the undeformed model. This model contains 10 spherical layers with 6 nodes in each layer. Up to 9 of these layers can be used to represent the waste container. One layer is required to represent the interface conditions between the waste container and the soil. The remaining internal nodes represent the soil. The interface between the soil and air is defined in this model by appropriate boundary conditions of convection and radiation applied to the surface nodes at the top of the model (nodes 3001-3009). This is in contrast to the method of using internal interface nodes to represent the air-to-container and air-to-soil interface.

Materials, temperatures and radii are defined via input for the spherical layers. The remaining nodes are assigned the appropriate material number and temperature representative of the soil. Twelve rows of cylindrical nodes are provided above the spherical section for simulating varying burial depths. Thicknesses of each row of nodes are defined via input to provide this capability. The radii of all cylindrical nodes and the thicknesses of cylindrical nodes in the side and base of the model are defined internally based on the outer radius of the spherical portion of the model.

2.1.4 Features and Limitations

The ESATA program contains the following calculational modeling features and limitations:

- Waste container representation - Three configurations are represented by internally generated models: An undeformed configuration in partial burial is represented by a 112 node model. A deformed configuration in partial burial is represented by a 252 node model. An undeformed configuration in varying depths of burial is represented by a 270 node model.
- Waste material representation - The waste material can be represented as a lumped representation of four constituents. Densities, specific heat and melting are proportioned by the weight of each constituent.

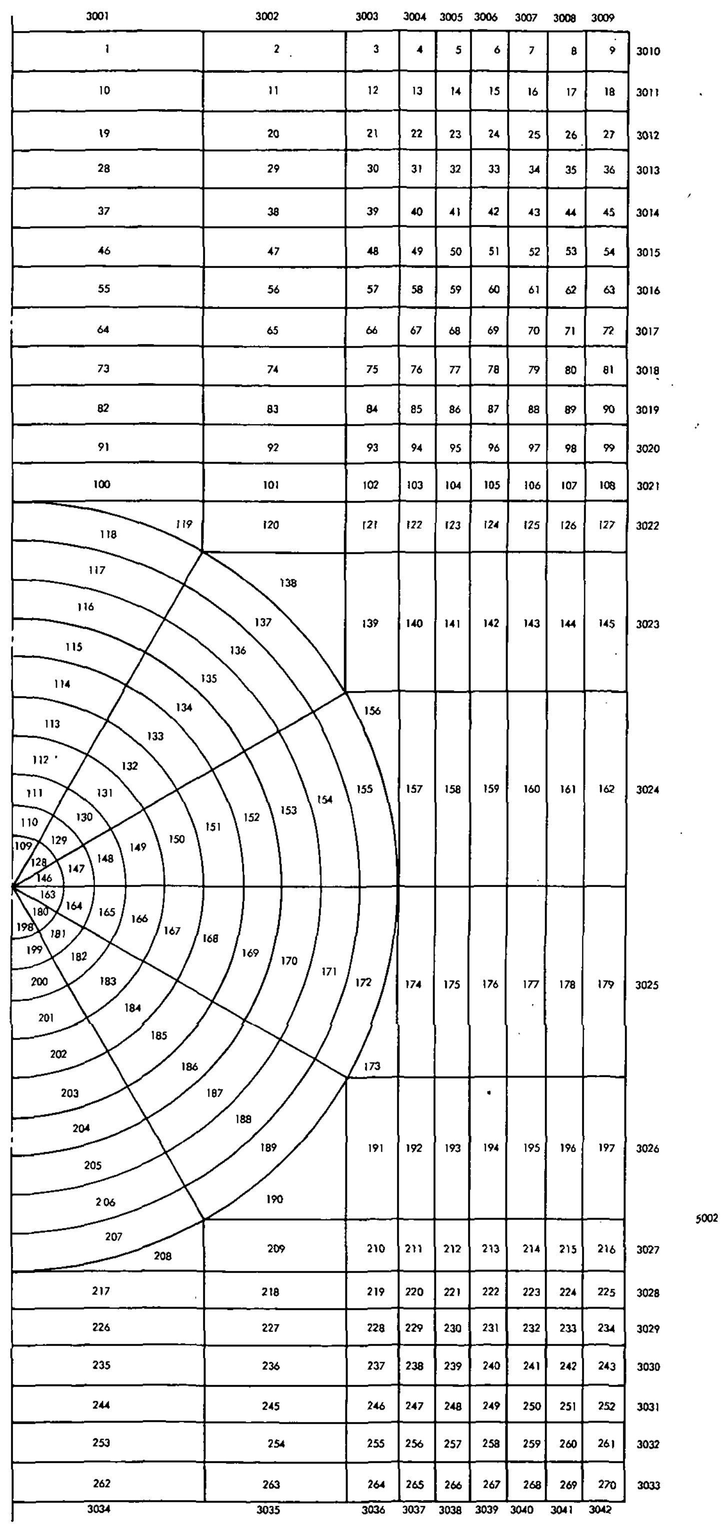

Figure 2-5. HTM-3 - Deep Buried Model

- Soil burial - The capability to analyze zero-to-full burial is provided for both the undeformed and deformed configurations. The undeformed configuration can also be analyzed for varying depths of burial.
- Deformation of waste container - Varying degrees of deformation can be treated via the input of row thickness with the usage of the deformed model.
- Geometry variations - Representation of the waste container and soil can be varied via the input of materials, temperatures and radii for each layer.
- Power level - The power level of the nuclear wastes is maintained constant at the prescribed input value. The heat sources are distributed among those nodes represented by the material that is designated as a heat source via input.
- Soil materials - Three soils are represented by properties in permanent storage in the code. Additional soils may be considered by the usage of normal TAP-A input.
- Component melting - The melting of all components is simulated by representing the heat of fusion as an effective specific heat.
- Component displacement - Displacement of components subsequent to melting is not simulated.
- Container to soil interface - Interface conditions of a variable contact coefficient, radiation gap or perfect soil contact can be represented via input.
- Hydride dissociation - The dissociation of LiH is treated on an average temperature basis. The heat of formation and increase in pressure buildup due to hydrogen release are simulated.
- Pressure response - In addition to hydrogen release from LiH dissociation, the release of helium from α emitters is treated. The subsequent change in pressure due to temperature changes are modeled.

- Stress analysis – A hoop stress and creep rupture analysis for the containment vessel is performed.

- Properties – Temperature dependent specific heats and thermal conductivities are stored internally for the commonly used materials. Additional properties may be specified by normal TAP-A usage.

- Time step accelerator – A procedure for increasing and decreasing the time increment during the transient is provided based on the number of iterations required for convergence at the previous time step.

- *Program restart – A program restart capability is provided. A matrix contain-*ing all the parameters required to restart the ESATA program at any point in the transient is output on tape. Computer time intervals for outputing or updating this matrix are specified as input data.

- Normal TAP-A input is available for geometry changes, material changes and temperature changes.

2.1.5 Input and Output Options

The quantity of input data required for the operation of any computer program becomes particularly important whenever the program is to be employed for analysis of many different configurations. To be effective in performing safety analysis of various post impacted nuclear power plant configurations, the analysis tool must be easy to use and the input data minimized. For this reason, generalized heat transfer models were developed for the ESATA program in order to minimize the input data required and thus maximize the usefulness of the program.

The general types of input data required are as follows:

- Variable Array Size for Geometry Related Parameters

- Titles

- Initial and Final Times, Time Increment and Convergence Criteria

- Set of Numbers to Identify Model Choice, Degree of Burial, Soil Selection and Temperature, Soil-to-Containment System Interface Condition, Total Heat Generation Rate, Soil Fusion Temperature, Amount of Emitting Fuel and Containment System Void Fraction
- Outer Radius, Material and Initial Temperature for Each Spherical Layer
- For Deformed Model Thickness of Each Layer in Deformed Base
- For Deep Burial Model, Thickness of Each Soil Layer above Spherical Portion of Model
- The Time During the Transient Period where Output Data is Required
- The Times (Computer Operation Time or Simulated Model Time) During Transient when all Data in Common Blocks are Placed on Restart Tape

A detailed description of the input data is presented in Appendix A. Computer output from an ESATA calculation consists of an edit of the input data, the results from the translation of the input data into the nodal point form required for the finite difference solution and the data output from the calculations. A detailed tabulation of this data is presented in Appendix A. The types of data output for each time step is presented below:

- Time Point in the Afterheat Decay Transient
- Temperatures for all System Components
- Power Level and Location of Heat Sources
- Percentage of Component Melting
- Heat Transfer from Containment Vessel to Soil and/or Air
- Internal Pressure, Containment Vessel Stress and Percent of Containment Vessel Life Used

2.2 SUBROUTINE DESCRIPTION

A general description of each subroutine is described in this section.

2.2.1 ESATA Main Program

This is the main program for the ESATA computer code. It contains the operational logic by which all primary subroutines of the program are called in the process of analyzing the temperature response of the reactor plant models. In addition, since ESATA is a variable dimensional program, the sizes for most matrices used in the calculations are computed based on the input data in this portion of the program. The titles and main program control variable for specifying the analysis option is also read in the main program.

2.2.2 TAP-A Functional Subroutines

The following subroutines were developed originally for TAP-A program usage and extended where necessary for usage compatible with the waste container post impact analysis option of the ESATA program. References 2, 3 and 4 contain additional information relative to the subroutines described below.

Subroutine INPUTT

These subroutines read input for performing the calculations. It consists of the input data required for the heat transfer models (HTM) contained in the program for performing the post impact analysis and the standard TAP-A data input routine.

Subroutine OUTPUT

This subroutine outputs the program data.

Subroutine POWER

This subroutine calculates internal heat generation summations and material capacitances. Heat generated at different nodes in the model are determined in subroutines HEAT and DISHYD.

These individual heating rates are summed in this subroutine on a per node basis. Heat capacitances for each node in the model are also computed. If a standard TAP-A run is made, this subroutine selects from the input data the heat generation rate for each node.

Subroutine STCALC

This subroutine calculates surface heat transfer coefficients and containment vessel surface temperatures.

Subroutine INOUT

This subroutine prints the input data, initial conditions, geometry data generated by HTMGEN, etc., or read in, and heat generation rates generated by HEAT.

Subroutine XLIN

This subroutine does a linear interpolation of independent and dependent variables to define the dependent variable based on the prescribed independent variable.

Subroutine CONDO

This subroutine calculates steady state and transient temperatures for each node in the model through solution of the finite difference equations. In addition, a procedure for varying the time increment during the afterheat decay transient is included. The procedure consists of monitoring the number of iterations required for solution convergence and doubling the time increment for the next calculational step whenever the number of iterations is less than 20.

2.2.3 HTM Generation Subroutine

The subroutine HTMGEN sets up the appropriate nodal geometry from the three nodal models described in Section 2.1.3 based on the input data option.

This subroutine sets up the following arrays which define the nodal geometry, nodal materials and initial temperatures:

VOL (i)	volume of node i
IJ (i, k)	index of node connected to node i by connection number k
IMAT (i)	material number of node i
OLDCON (i, k)	the length to area ratio for node i and connection number k.
IDEMK (i, j)	define use of primary or secondary conductivity
SAREA (i)	surface area for surface to boundary connections
IJS (i)	node index for internal or boundary node connected to node i
H (i)	surface heat transfer coefficients
ST (i)	surface node temperature
BT (i)	boundary node temperature
T (i)	internal node temperature

2.2.4 Heat Generation Subroutines

The general heat transfer calculation option for normal heat generation rates are supplied to the code via input data for each node. For the waste container post impact analysis option, heat generation rates for each node are calculated internally. There are two sources for heat generation in the ESATA program. One source is the nuclear waste decay power which is calculated in HEAT for each heat source node based on the input of the total decay power level. The other source is the heat generated or absorbed due to hydride dissociation which is calculated in the subroutine DISHYD described in Section 2.2.7. A general description of the HEAT subroutine is presented below. Energy absorption associated with phase changes are simulated in the capacitance calculation by effective specific heats.

Subroutine HEAT

This subroutine distributes the total heat generation rate attributed to the radioactive nuclear materials specified via input among all nodes designated to contain these materials. The total power level is distributed on a volume weighted basis. A material number is inputted which is to represent the heat source. For consideration of the composite material representing the four constituents, this number is 49. All nodes containing that material are assigned a heat generation rate. At the present time, the decay of power with time is neglected because of the relatively short time period in which the impact analysis is performed.

2.2.5 Surface Heat Transfer Subroutine

The subroutine SURFQ calculates the rate of heat transfer from the waste container to the environment at time steps when the output data is printed. The heat transfer rate from the container is broken into heat conducted to the soil, radiated to air, and convected to air. The sum of these terms are compared to the total heat generation rate.

2.2.6 Melting Subroutine

The TMPCAL subroutine performs the function of simulating the heat of fusion when a material melts or fuses. The heat of fusion (stored in block DATA for 20 materials) is modeled by an effective specific heat defined over a finite temperature range.

$$C_P = \frac{H_{F_g}}{\Delta T} \quad \text{where } \Delta T = 50^{\circ}R$$

After a temperature convergence is obtained in CONDO for a particular time step, the temperatures of all nodes assigned one of the above materials are compared to their melting point temperature plus the band of $50^{\circ}R$ above the melting used to simulate the phase change. The temperature of a node is corrected based upon the percent of melting, the previous calculated temperature, and the present temperature for a node relative to the $50^{\circ}R$ melting band.

The fraction of melting is:

$$X_{mel} = \frac{(T - T_{mp})}{\Delta T}$$

where

T = the corrected temperatures

T_{mp} = the melting point temperature

X_{mel} = fraction of melting

When this fraction is 1.0, melting is completed. Equations are defined to simulate the correct value of H_{fg} irrespective of the number of time steps to go through the melting and irrespective of the magnitude of the old and new node temperature relative to the melting band. (Typical equations and approach presented in Appendix D of Reference 2)

In addition to the single component melting, this subroutine calculates melting of the four constituents in the waste material composite. The composite material will go through the four melting points in the following order based on temperature level:

Aluminum
LiH
Copper
Waste Products

2.2.7 Hydride Dissociation Subroutines

Subroutine DISHYD

The procedure for simulating the dissociation and recombination of lithium hydride is based on the following assumptions:

- Pressure gradients in the system are neglected.
- Perfect gas law assumed.
- The heat of reaction is simulated.

This subroutine first defines at any time step an average temperature of the hydride material. The equilibrium pressure of H_2 in the presence of LiH is then calculated based on the average hydride temperature. The total number of hydrogen moles that can be released by dissociation is then calculated based on the equilibrium pressure, average temperature and total void volume using the perfect gas law.

The effect of dissociation on the individual hydride nodes is then considered. The number of moles of hydrogen released from each node is calculated by the perfect gas law using the equilibrium pressure, the local node temperature, and void volume assigned to the node. The number of moles of H_2 released from a node is limited to the maximum number available for that node. The fraction of dissociation occurring during the time step is calculated and a heat generation rate is calculated based on this fraction of dissociation, the node mass and the heat of reaction.

The number of moles released from each node is summed and compared to the total number that can be released. If these two quantities do not agree (resulting from completion of dissociation locally) the amount of dissociation for each node is corrected by the ratio of the two totals.

Subroutine INTHYD

This subroutine initializes arrays denoting the location of hydride materials, the amount of hydrogen available and the local void volumes.

2.2.8 Pressure and Stress Subroutine

Subroutine PRESUR

This subroutine calculates the pressure buildup inside the containment vessel, the maximum hoop stress level of the containment vessel and the containment vessel percent life used on a creep rupture basis.

Two components are considered in the pressure buildup; namely, the helium released from α emitters and hydrogen released from hydride dissociation. This subroutine takes the vapor masses calculated in other subroutines and calculates the partial pressures of each component based on the perfect gas law (Appendix E of Reference 2). The total pressure is calculated and used to calculate a hoop stress based on the radius and thickness of the containment vessel. The Larsen Miller parameter is calculated based on SS-316 creep rupture data and the maximum containment vessel temperature using the following:

$$(60 - LM)^{0.496} - (\mathrm{Log}_{10}\sigma)^{1.2} = 1.2 = 0$$

where

LM	=	Larsen-Miller parameter
	=	stress level

The time to failure is computed from the standard Larsen-Miller equation

$$LM = (T + 460)(a + \mathrm{Log}_{10}t) \times 10^{-3}$$

where

T	=	temperature of the vessel in $^{\circ}F$
a	=	experienced constant having a value of 20 for the 316 stainless steel material
t	=	time to failure at the applied stress (σ) level

The percent of life used in each time step is calculated based on the time increment divided by the time to failure (t). The percent of life used is summed to determine the total used-up for fraction of life. When this fraction equals 1, rupture is assumed to occur.

2.2.9 Property Data Subroutines

Several subroutines and functions are used to store and calculate property data and calculate effective property data to simulate internal interface conditions. Appendix B presents the detailed data and equations.

Subroutine VARK

This subroutine defines the thermal conductivity based on materials defined in Table 2-1 for each node and calculates the thermal conductance between each node in the model. It calls the PROTK functions described below. VARK contains the logic to calculate effective conductivities for the soil to containment vessel contact coefficient, vessel to air interface of radiation and natural convection, and air-to-air nodes. It assigns high or low conductivities for one-dimensional heat transfer paths through materials or across interfaces. It also assigns a thermal conductivity of 17 Btu/Hr-Ft-^{o}F for the composite waste material.

Function PROTK

This subroutine stores thermal conductivity data versus temperature for 14 materials pertinent to the post impact of the waste container. It does a linear interpolation of this data to define a thermal conductivity for a prescribed material and temperature.

Block DATA

This subroutine stores density, melting point temperature and the heat of fusion for 14 basic materials.

Function PROCP

This subroutine stores specific heat data versus temperature for 14 materials. It does a linear interpolation of this data to define a specific heat for a prescribed material and temperature.

Subroutine CPCAL

Defines effective specific heat and density for all materials (components) not defined by basic material properties; for example, defines effective properties for the composite waste material. The capacitance of the waste material is mass weighted based on the capacity of each constituent simulated in the material and the fraction of the mass of each material over the total mass of the component.

TABLE 2-1

MATERIALS STORED IN ESATA

MATERIAL NUMBER	DESCRIPTION
1	Waste Products
2	Aluminum
3	Stainless Steel 316
4	Lithium Hydride
5	Tungsten
6	Graphite
7	Teflon
8	Thermal Switch Insulation
9	Lithium
10	Coastal Plains Soil
11	Granite Detrital
12	Laterite Soil
13	Water
14	Copper
21-40	Temperature Dependent and Constant Properties that can be Input by User via TAP-A Standard Input
41	1-d High K Axially
42	1-d High K Radially
43	2-d High K
44	Vessel-to-Soil Interface
45	Vessel-to-Air Interface
46	Air Nodes
47	Vessel-to-Water Interface
48	Dissociated LiH
49	Homogeneous Waste Product Composite

3.0 TASK II - HEAT TRANSFER CALCULATIONS

For this study, 21 cases were analyzed. These cases considered variations in container design, power levels, degree of burial, soil conditions and degree of deformation. A single general waste container was defined which is described in Section 3.1. A basic assumption was made that all reentry protective materials were separated from the container after impact. A description of the 21 cases is presented in Section 3.2. Three cases were selected for detailed analysis which are described in Section 3.3. Pertinent data from all 21 cases are described in Section 3.4. Results are described in Section 3.5.

3.1 GENERAL DESCRIPTION OF WASTE CONTAINERS

The general configuration of the waste containers considered in this study is shown schematically in Figure 3-1. The containers consisted of spherical layers of alternate materials. The innermost material was the nuclear waste material. For this study, this material was analyzed as a homogeneous composite of aluminum, LiH, copper and waste products. The waste material was enclosed by a thin layer of tungsten shielding. LiH shielding was placed adjacent to the tungsten and the shield and waste material package was enclosed by a SS-316 container. Reentry shielding materials such as graphite and teflon which were initially protecting the container were assumed to be separated from the container for this post impact analysis.

3.2 DESCRIPTION OF CASES

Tables 3-1 and 3-2 summarizes the characteristics of the 21 cases analyzed in this study. Included in these tables are descriptions of the power level, post impact configuration, degree of burial, geometry, soil conditions, initial temperatures, initial pressures and fuel weights. These cases were selected to provide several comparisons including:

- The Effect of Power Level in a Single Geometry
- The Effect of Partial Burial Versus Deep Burial
- The Effect of Deformation in Partial Burial Conditions

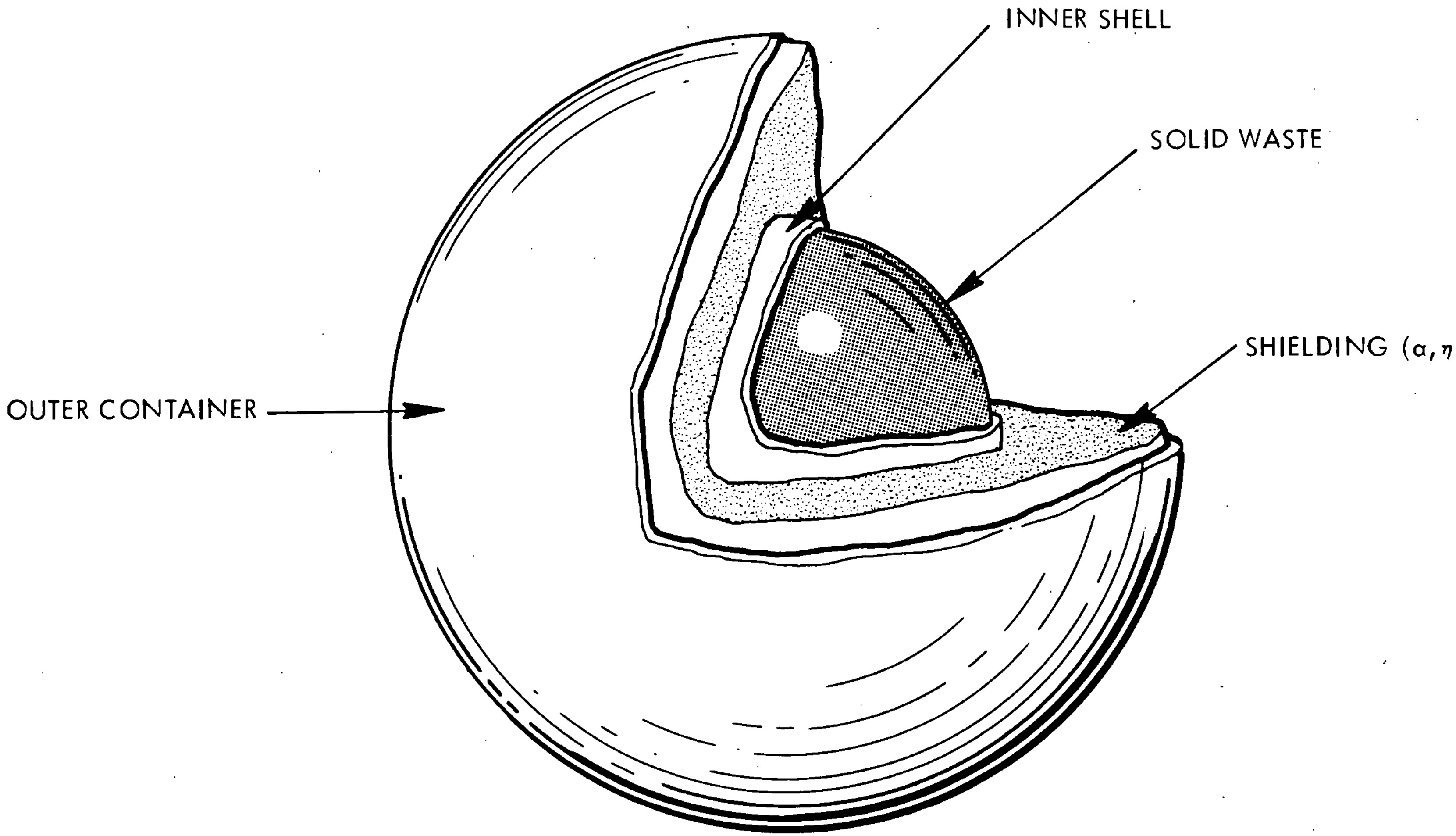

Figure 3-1. Radioactive Nuclear Waste Container Configuration

TABLE 3-1

DEFINITION OF TWENTY-ONE HEAT TRANSFER MODELS

CASES	POWER, KW	IMODEL	IBURY, % or Ft to Base	r_1 - radius - in. - material (fuel)	r_2 - radius - in. - material (w)	r_3 - radius - in. - material (LiH)	r_4 - radius - in. - material (ss)	r_5 - radius - in. - material (soil)	t - fuel - in.	t - tungsten - in.	t - LiH - in.	t - Stain. - in.	t - soil - in.	Soil Material	Amb. Temp. ^{o}R	C. V. Temp. ^{o}R	CL Fuel Temp. ^{o}R	Initial Press. PSI	Void Fraction - %	Soil Temp. - ^{o}R	REMARKS
1	24	Undef.	37.5%	18 in.	19.46	24.26	25.26	131.3						Coastal Plains	530	1660	1460	25	10%	530	Check Cases
2	24	Dp. Bur		↓	↓	↓	↓	↓						↓	↓	↓	↓	↓	↓	↓	
3	24	Def.	0	↓	↓	↓	↓	↓		13.5	1.46	3.6	1.0	↓	↓	↓	↓	↓	↓	↓	
4	1.5	Dp. Bur	22	8	8.9	11.5	12.0	60.0						↓	↓	↓	↓	↓	↓	↓	Low Power Case
5	5	↓	30	9.76	11.56	14.4	15.4	75.0						↓	↓	↓	↓	↓	↓	↓	1 of 3 spheres for hi earth orbit mod.
6	7	↓	30	11.27	12.67	16.67	17.67	90.0						↓	↓	↓	↓	↓	↓	↓	Solar Escape Mod.
7	10	↓	30	↓	↓	↓	↓	↓						↓	↓	↓	↓	↓	↓	↓	Solar Escape Mod. Hi Power
8	7	Def.	0	↓	↓	↓	↓	↓		7.6	9.5	2.67	1.0	↓	↓	↓	↓	↓	↓	↓	Solar Escape Mod. on Ground
9	7	Def.	Nodes 171	↓	↓	↓	↓	↓						↓	↓	↓	↓	↓	↓	↓	Solar Escape Mod. Partial Burial
10	15	Dp. Bur.	33	18	19.46	24.26	25.26	131						↓	↓	↓	↓	↓	↓	↓	Most Econ. Model Hi Earth Orbit - Low Power
11	20	↓	↓	↓	↓	↓	↓	↓						↓	↓	↓	↓	↓	↓	↓	Medium Power
12	30	↓	↓	↓	↓	↓	↓	↓						↓	↓	↓	↓	↓	↓	↓	Hi Power
13	24	Def.	Node 171	↓	↓	↓	↓	↓		12.0	1.0	3.21	1.0	↓	↓	↓	↓	↓	↓	↓	Partial Burial
14	24	Dp. Bur.	33	↓	↓	↓	↓	131						Podzol	↓	↓	↓	↓	↓	↓	Soil Investigation
15	24	↓	6	↓	↓	↓	↓	↓						↓	↓	↓	↓	↓	↓	↓	Surface Temp. Investigation
16	24	↓	9	↓	↓	↓	↓	↓						↓	↓	↓	↓	↓	↓	↓	↓
17	24	↓	14	↓	↓	↓	↓	↓						↓	↓	↓	↓	↓	↓	↓	↓
18	1.5	↓	22	8	8.9	11.5	12.0	60						↓	↓	↓	↓	↓	↓	↓	↓
19	5	↓	30	9.76	11.56	14.4	15.4	75						↓	↓	↓	↓	↓	↓	↓	↓
20	7	↓	30	11.27	12.67	16.67	17.67	90						↓	↓	↓	↓	↓	↓	↓	↓
21	10	↓	30	11.27	12.67	16.67	17.67	90						↓	↓	↓	↓	↓	↓	↓	↓

TABLE 3-2

WEIGHT SUMMARY (LBS)

Case	Fuel	LiH	Copper	Aluminum
1	800	280	1650	500
2	800	280	1650	500
3	800	280	1650	500
4	50	33.5	201	60.8
5	167	43.5	260.6	78.8
6	233	68.2	409	124
7	300	64.6	388	117
8	233	68.2	409	124
9	233	68.2	409	124
10	500	303	1815	549
11	666	293	1760	532
12	900	281	1683	509
13	800	280	1650	500
14	800	280	1650	500
15	800	280	1650	500
16	800	280	1650	500
17	800	280	1650	500
18	50	33.5	201	60.8
19	167	43.5	260.6	60.8
20	233	68.2	409	78.8
21	300	64.6	388	124

- The Effect of Burial Depth
- Comparison of Alternate Designs
- The Effect of Soil Property Variations

Two soils were selected from a group of nine soils tested by the National Bureau of Standards[5] for Sandia Corporation for consideration in these analyses. One soil was coastal plains soil which is typical of well-weathered soil representative of approximately 15% of the total land area of the world. In addition to being a common soil, this soil was selected based on having a "typical" thermal conductivity in comparison to the other soils. The other soil considered was Podzol soil which is leached organic soil of woodland regions of temperate zones of the world which comprise about a quarter of the total land area of the world. In comparison to coastal plains soil, this soil had a higher thermal conductivity and higher temperature level for fusing, thus providing a trade-off in soil property variations. The coastal plains soil was used in the first 13 cases and the podzol soil was used in the remaining 8 cases.

The first three cases were check cases for the three models (partially buried undeformed model, deep buried undeformed model and a non-buried deformed model). A reference design, consisting of a four-foot diameter container with 800 pounds of nuclear waste material producing 24 KW of power was used for these cases. These cases were analyzed in detail to determine the operationability of the modified ESATA code and were compared to determine the effects of deformation and degree of burial. Cases 4-7 compared 4 container designs ranging in diameter from 24 inches to 35 inches and in power from 1.5 KW to 10 KW. The containers were assumed to be undeformed and deeply buried (22-30 feet). These cases provided a comparison of high earth orbit modules and solar escape modules. Cases 8 and 9 considered the solar escape module (case 6 with 7 KW of nuclear wastes) in a deformed configuration with zero and partial burial. Cases 6, 8 and 9 provided trade-offs in deformation and degree of burial.

Cases 10-12 considered the reference design (4 foot diameter container) with variations in nuclear waste material weight and power level ranging from 15-30 KW. The container was assumed to be undeformed and deeply buried. Cases 2, 10, 11 and 12 provided a comparison of power level in a single container design. Case 13 considered the reference design in a deformed configuration and partially buried. Cases 2 and 13 provided another comparison of degree of burial for the deformed configuration. Case 14 considered the undeformed reference design deeply buried in podzol soil and in comparison to case 2 indicated the effects of soil property variation. Cases 15 - 17 considered the reference design in an undeformed configured burial to varied depths to provide a trade-off of burial depths. Cases 18-21 were a repeat of cases 4-7 deeply buried in podzol soil. This set of cases provided an evaluation of the alternate designs exposed to deep burial in a more conductive soil than cases 4-7.

3.3 DETAILED ANALYSIS OF THREE WASTE CONTAINER CONFIGURATIONS

Three cases were selected for detailed evaluation and analysis. Two of the cases represented the undeformed reference design in partial (case 1) and deep (case 2) burial in coastal plains soil. The third case considered the 7 KW solar escape module deeply buried in podzol (case 20).

3.3.1 Case 1 Results

Case 1 considered the partial burial (37.5% diametral burial) of an undeformed 4 foot diameter 24 KW waste container. The general definition of this case was shown in Tables 3-1 and 3-2. For this case, the HTM-1 model shown in Figure 2-2 was used to perform the analysis. The nodes were assigned the radii and materials indicated in Table 3-3. Intimate contact between the soil and container was assumed.

Case 1 was run for a total of 2 million seconds. Figure 3-2 is a plot of the axial temperature profile for the fuel (center), base of the tungsten shield, base of the containment shell and the soil adjacent to the base of the containment shell.

The initial temperature of the surface of the waste container was higher than the fuel due to the large external heating rates during reentry. After impact, the heat load is that due to the

TABLE 3-3

CASE 1 RADII AND MATERIALS

Undeformed Model - Figure 2-2 - 37.5% Burial (Diametrol %)

Layer	Nodes	Outer Radius (Inches)	Material
1	1-8	3.	Composite Fuel
2	9-16	9.	Composite Fuel
3	17-24	18.	Composite Fuel
4	25-32	19.46	Tungsten
5	33-40	20.66	LiH
6	41-48	21.86	LiH
7	49-56	23.06	LiH
8	57-64	24.26	LiH
9	65-72	25.26	SS-304
10	73-80	26.26	Air/Soil Interface
11	81-88	32.8	Air/Coastal Plains Soil
12	89-96	52.5	" " " "
13	97-104	85.3	" " " "
14	105-112	131.3	" " " "

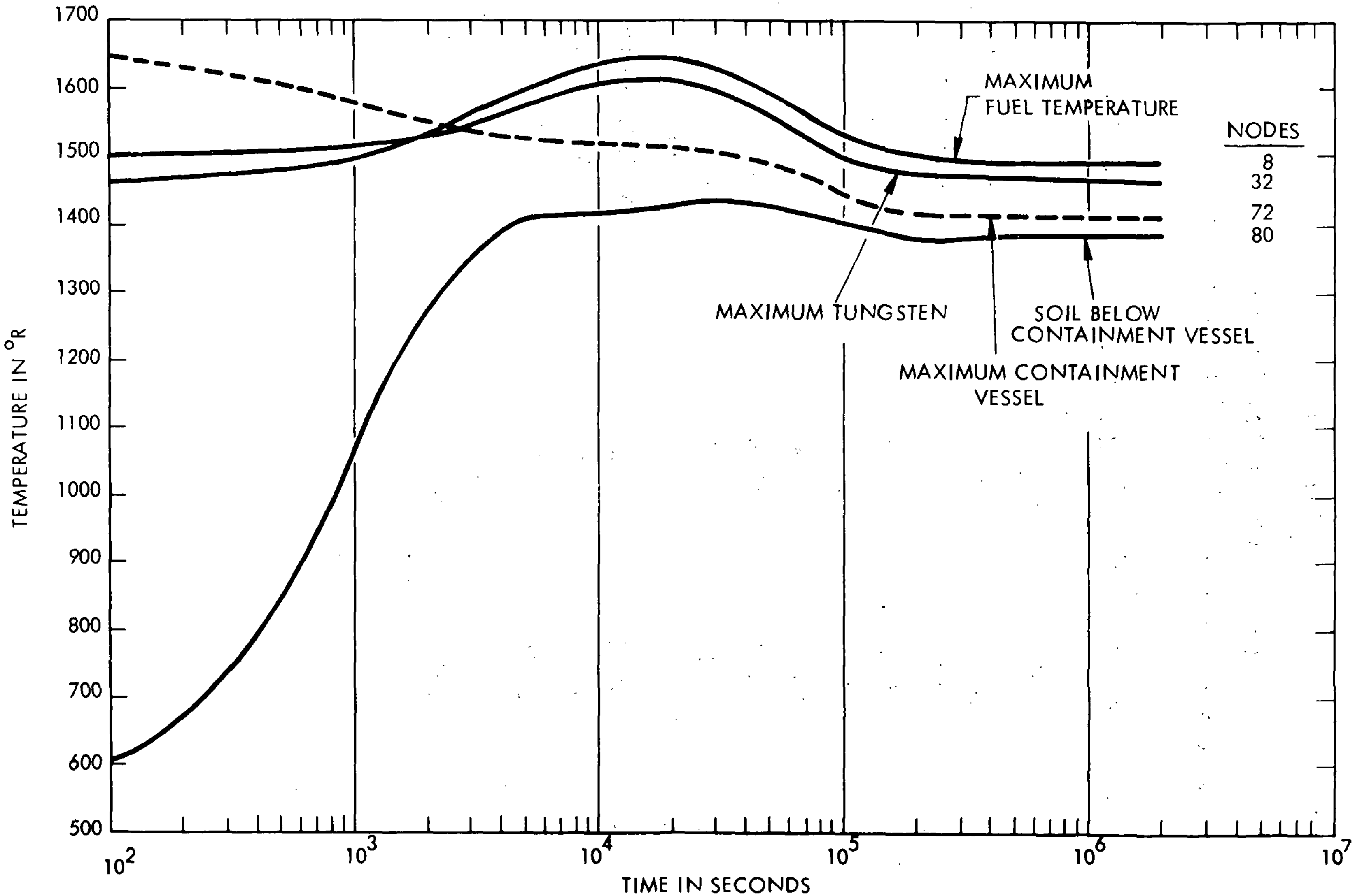

Figure 3-2. Axial Temperature Profile for Case 1 Waste Container

waste products; therefore, the temperature gradient reversed during the transient. The containment vessel surface gradually dropped from 1660°R to 1440°R as the soil at the base heated to 1200°R. The fuel increased from 1460°R to 1660°R in the first 15,000 seconds and then followed the gradual cooling of the containment surface after a sufficient thermal gradient was established in the system to conduct away the heat energy of the waste products. After 1 million seconds, the system had reached a steady state condition. For this case, with only 37.5%, burial along the circumference, no melting of the soil occurred.

Figure 3-3 is a plot of the temperature response radially for the fuel, tungsten shield, and containment shell in a section exposed to air. This figure also indicates the reversal of the temperature gradient in the waste container during the transient. Because of the greater heat rejection capability to air by convection and radiation, the containment vessel cooled to a level of 1000°R which was 300°R lower than at the bottom. Since most of the energy was being conducted to the top, the temperature drop across the LiH radially was approximately 300°R which was much greater than in the base. A steady state temperature profile was established after approximately 300,000 seconds.

Figure 3-4 presents a breakdown of the heat dissipation to the environment and compares the heat dissipation rate to the internal heat generation rate. Due to the initial temperature conditions upon impact induced by the reentry heating, the container is cooled by the environment significantly as shown in the temperature plots. The total heat dissipation rate from the container is approximately 149 Btu/sec 100 seconds subsequent to impact compared to a heat generation rate of 22.75 Btu/sec. The major contribution to the heat dissipation initially was radiation to ambient (106 Btu/sec). A surface emmissivity of 0.8 with a view factor of 1.0 was assumed for this calculation. The contribution of natural convection to the ambient was 24 Btu/sec at 100 seconds, and the remaining 19 Btu/sec was by conduction to soil. As the transient progressed the waste products and containment system cooled to lower steady state temperature levels than initially due to sufficient exposure to the ambient. The heat dissipation rate therefore gradually approached the heat generation rate of the waste products. After

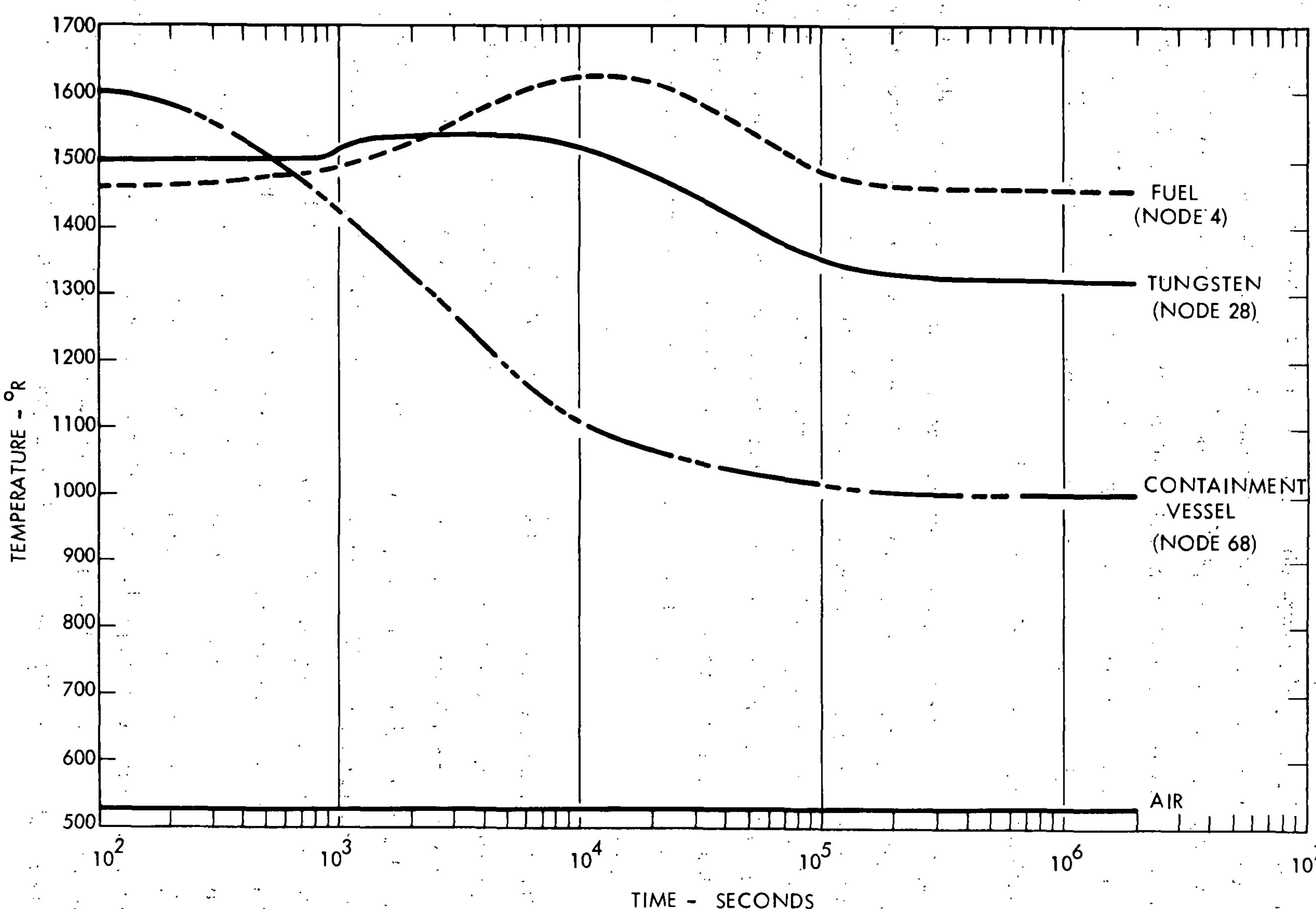

Figure 3-3. Radial Temperature Profile for Case 1 Waste Container

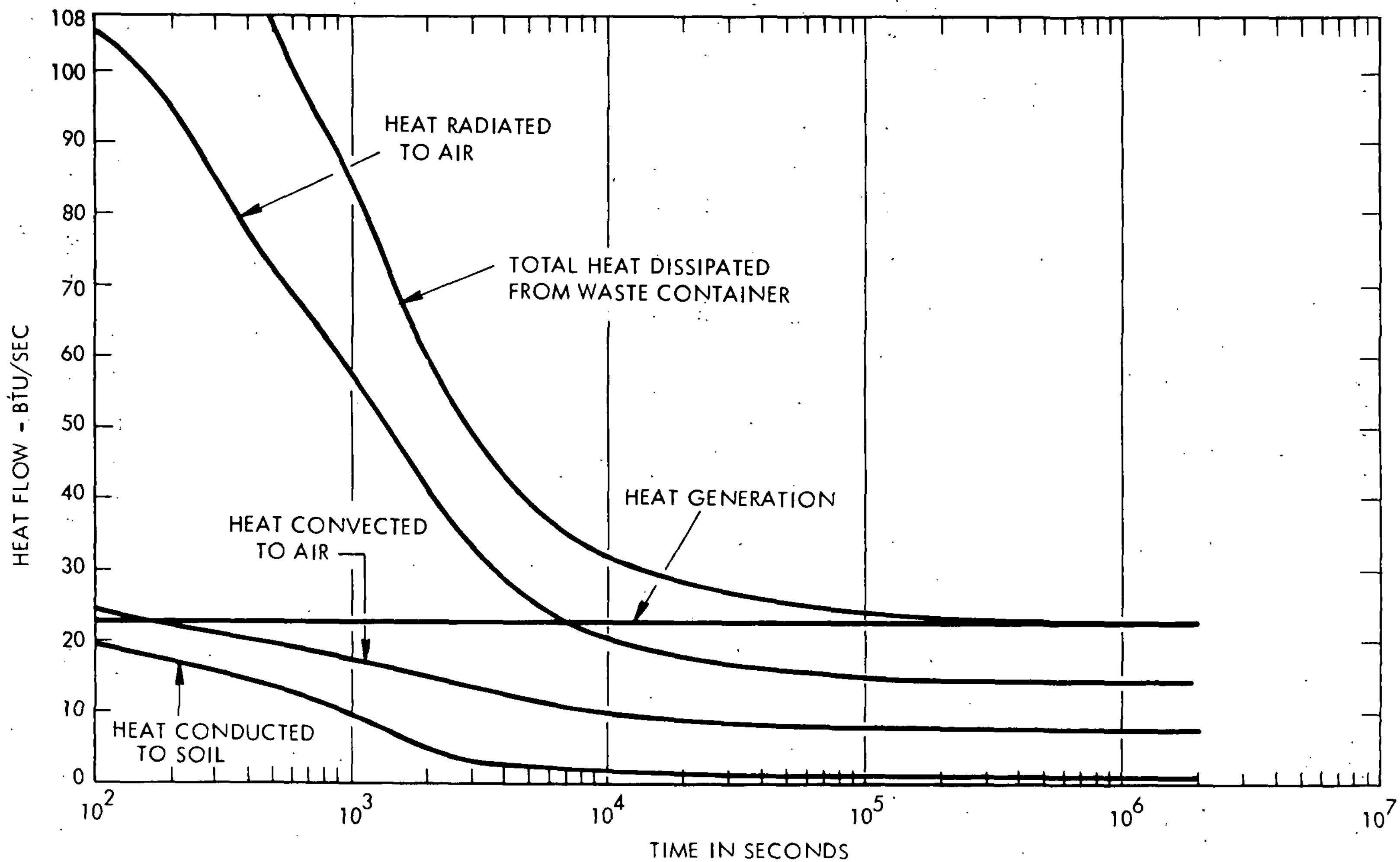

Figure 3-4. Heat Generation and Dissipation for Case 1

300,000 seconds, the distribution of the heat dissipation was 14.3 Btu/sec by radiation to air, 7.7 Btu/sec by natural convection to air and 0.8 Btu/sec by conduction to the soil.

The internal pressure response for this case is shown in Figure 3-5. Because the system cooled to a lower steady state condition, the internal pressure dropped from a 25 psi initial pressure to approximately 21 psi. For this case, LiH dissociation was not considered.

Figure 3-6 is a plot of the hydrogen equilibrium pressure for LiH as a function of LiH temperature. A peak LiH temperature of 1600°R was indicated for case 1 by the peak tungsten temperature in Figure 3-2. As shown in Figure 3-6, the hydrogen equilibrium pressure is much less than 1 psi thus the contribution of hydride dissociation to the pressure response is negligible for this case.

Figure 3-7 is a plot of the circumferential temperature profile in the containment vessel and tungsten shield at steady state. Because of the low thermal conductivity of the soil, the base of the containment vessel exposed to the soil reached a higher temperature than the upper portion exposed to the air. Out of the 22.75 Btu/sec (24 Kw) total heat generated by the waste products, 22 Btu/sec were being dissipated to the air and the remainder to the soil. The higher heat load to the air resulted in a 300°F drop radially across the LiH in the top region versus a 50°F radial drop in the base.

3.3.2 Case 2 Results

Case 2 considered the deep burial (19 feet to base of sphere) of the reference configuration considered in Case 1. The HTM-3 model, shown in Figure 2-4, was used for this analysis. The general conditions for this case are shown in Tables 3-1 and 3-2. The nodes were assigned materials and radii indicated in Table 3-4.

Figure 3-8 shows the temperature response of the fuel center, tungsten, containment vessel, and the soil one inch below the container. This temperature response represents a slice in the system from the fuel center vertically downward to below the base of the containment system.

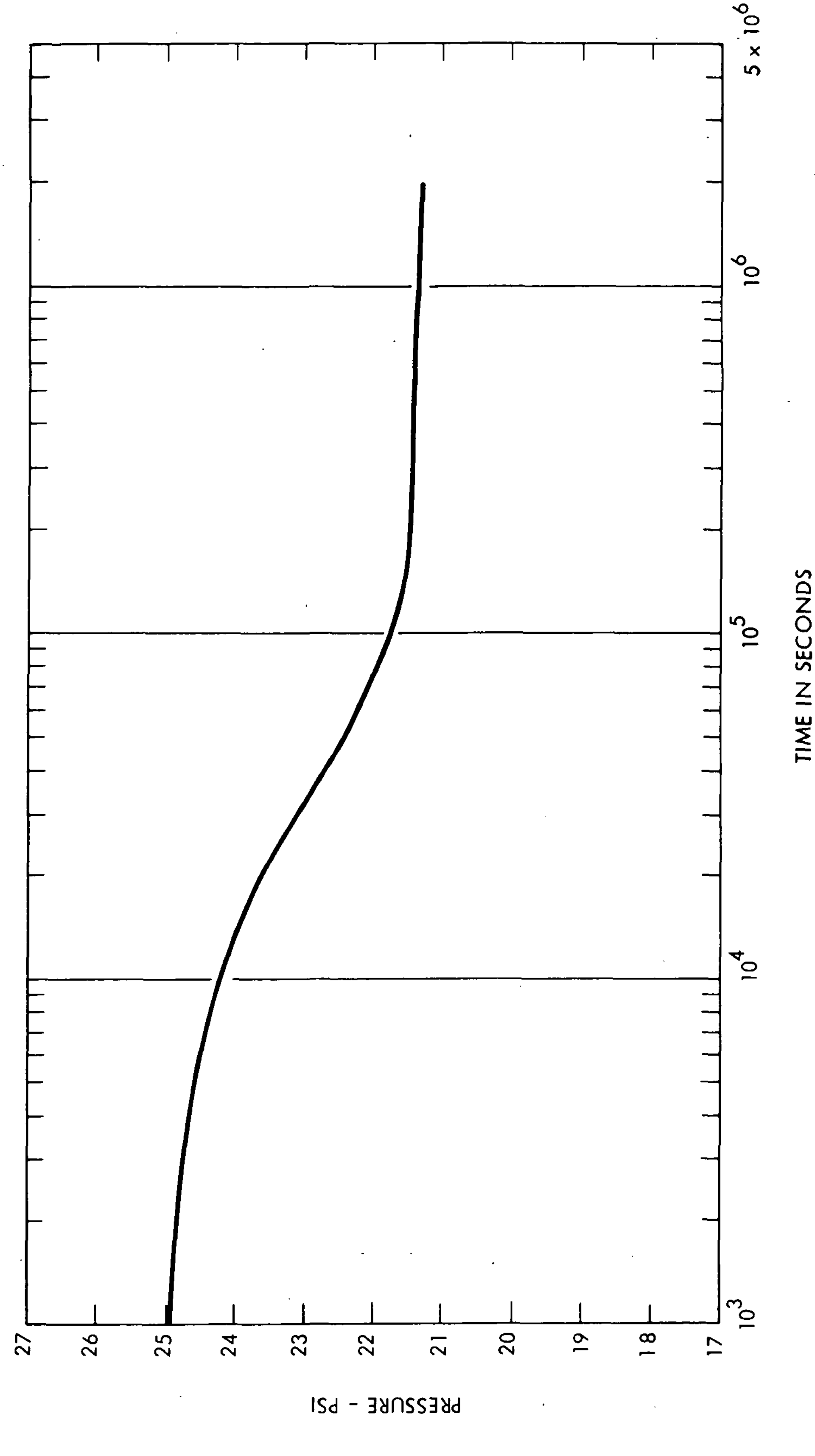

Figure 3-5. Internal Pressure Response for Case 1

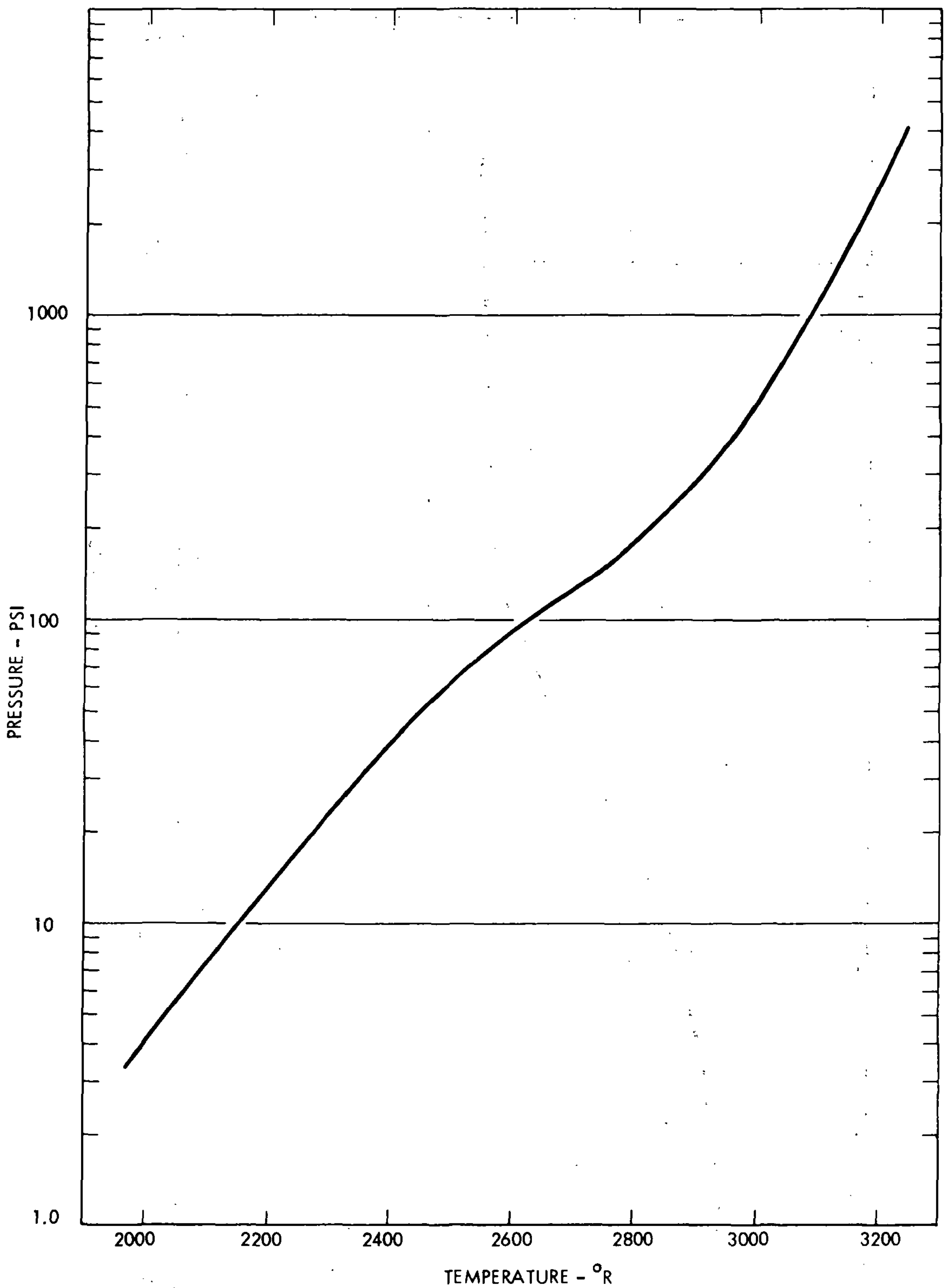

Figure 3-6. Hydrogen Equilibrium Pressure for LiH

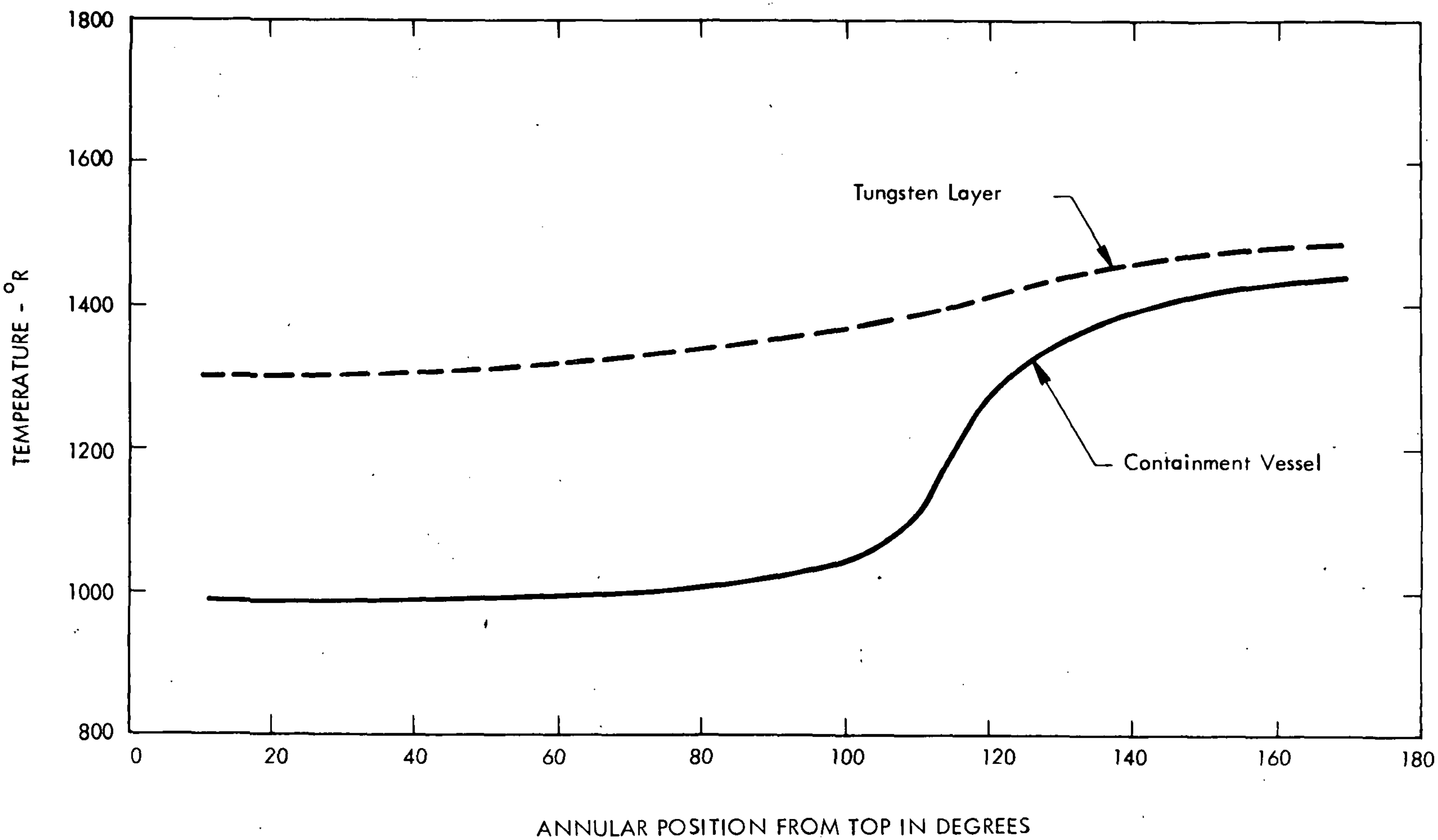

Figure 3-7. Comparison of Tungsten Layer and Containment Vessel at 2×10^6 Sec. for Case 1

TABLE 3-4

CASE 2 RADII THICKNESSES AND MATERIALS

Deep Burial Model (Figure 2-4)

A. Spherical Section

Layer	Nodes	Outer Radius (Inches)	Material
1	109,128, 146,163, 180,198	9	Fuel
2	110-199	18	Fuel
3	111-200	19.46	Tungsten
4	112-201	21.06	LiH
5	113-202	22.66	LiH
6	114-203	24.26	LiH
7	115-204	25.26	SS-304
8	116-205	26.26	Coastal Plains Soil
9	117-206	27.26	" " "
10	118-207	28.26	" " "

B. Upper Cylinder Section (All coastal plains soil)

Row	Nodes	Thicknesses (In.)	Layer	Nodes	Outer Radii(In.)
1	1-9	18.	1	1,10,19--,100	14.1
2	10-18	18.	2	2,---,101	24.5
3	19-27	18.	3	3,---,102	28.5
4	28-36	18.	4	4,---,103	32.5
5	37-45	18.	5	5,---,104	42.2
6	46-54	18.	6	6,---,105	61.3
7	55-63	18.	7	7,---,106	98.
8	64-72	18.	8	8,---,107	171.5
9	72-81	15.	9	9,---,108	325.9
10	82-90	12.			
11	91-99	6.			
12	100-108	3.			

TABLE 3-4 (Continued)

C. Center Cylindrical Section (All Coastal Plains Soil)

Row	Nodes	Thicknesses (In.)	Layer	Nodes	Outer Radii (In.)
1	119-127	3.8	4	122,140,---,211	32.5
2	138-145	10.3	5	123,---,212	42.2
3	156-162	14.1	6	124,---,213	61.3
4	173-179	14.1	7	125,---,214	98.
5	190-197	10.3	8	126,---,215	171.5
6	208-216	3.8	9	127,---,216	325.9

D. Bottom Cylindrical Section (All Coastal Plains Soil)

Row	Nodes	Thicknesses (In.)	Layer	Nodes	Outer Radii (In.)
1	217-225	4.2	1	217,226,---,262	14.1
2	226-234	9.8	2	218,---,263	24.5
3	235-243	19.0	3	219,---,264	28.5
4	244-252	36.8	4	220,---,265	32.5
5	253-261	73.5	5	221,---,266	42.2
6	262-270	154.3	6	222,---,267	61.3
			7	223,---,268	98.
			8	224,---,269	171.5
			9	225,---,270	325.9

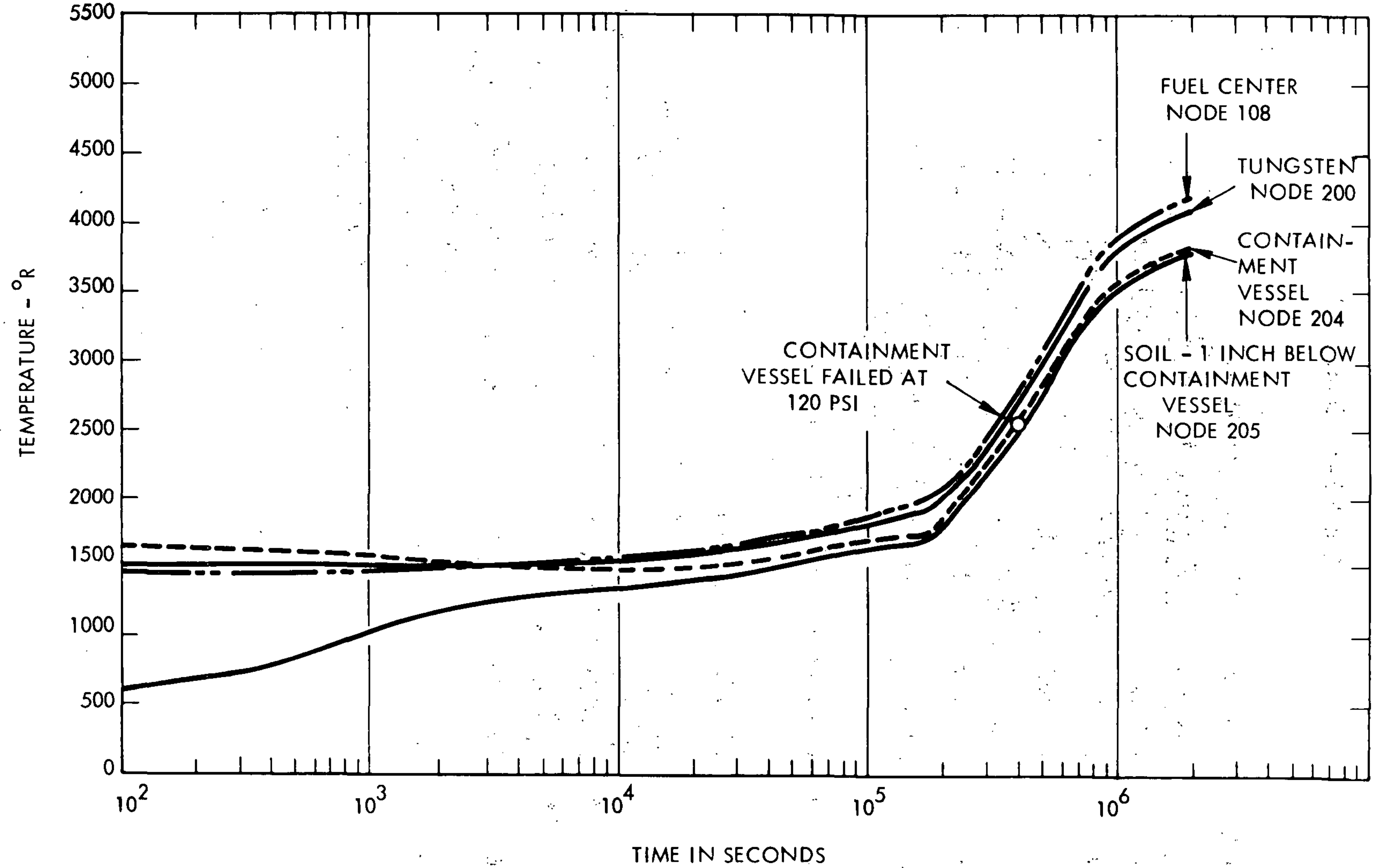

Figure 3-8. Axial Temperatures in Waste Container for Case 2 (HTM-3 with LiH Dissociation)

Because of the relative low thermal conductivity of the coastal plains soil considered for this case, the waste products and containment system rose to temperatures in excess of 3500°R. During the initial period of the transient, the temperature gradient in the waste container was reversed as evidenced in Case 1. This was due to the initial temperature drop from the containment vessel to the soil being sufficiently large to result in heat dissipation rates much greater than the heat generation rate. The surface of the containment system and the soil surface converged in temperature, therefore, delayed the heating of the waste products. After approximately 30,000 seconds, the aluminum and LiH mixed in the waste products and the LiH between the tungsten and containment vessel started to melt further delaying the response of the system. After 150,000 seconds, all the LiH was molten and the system started to heat at a faster rate. During the subsequent period of time, the LiH started to dissociate in sufficient quantity to influence the pressure response. At 400,000 seconds (4.6 days) the containment vessel was predicted to have a stress rupture failure. At this point in time, the peak containment vessel temperature was 2500°R, and the internal pressure was 120 psi.

The waste container was buried to a sufficient depth such that the earth's surface did not influence the flow of heat in the container and all heat flow was in the radial direction.

This is illustrated in Figure 3-9, which is a plot of the circumferential temperature profile in the fuel, tungsten and containment vessel after 2 million seconds. A plot of the model centerline temperature profile from the surface of the earth to the base of the waste container is shown in Figure 3-10 at 2 million seconds into the transient. This figure indicated that the soil temperatures were at ambient conditions over the first 10 feet below the surface. At greater depths, a temperature gradient was established in the soil. This result indicated that significantly less burial depths would not alter the response of the waste container to any significant degree.

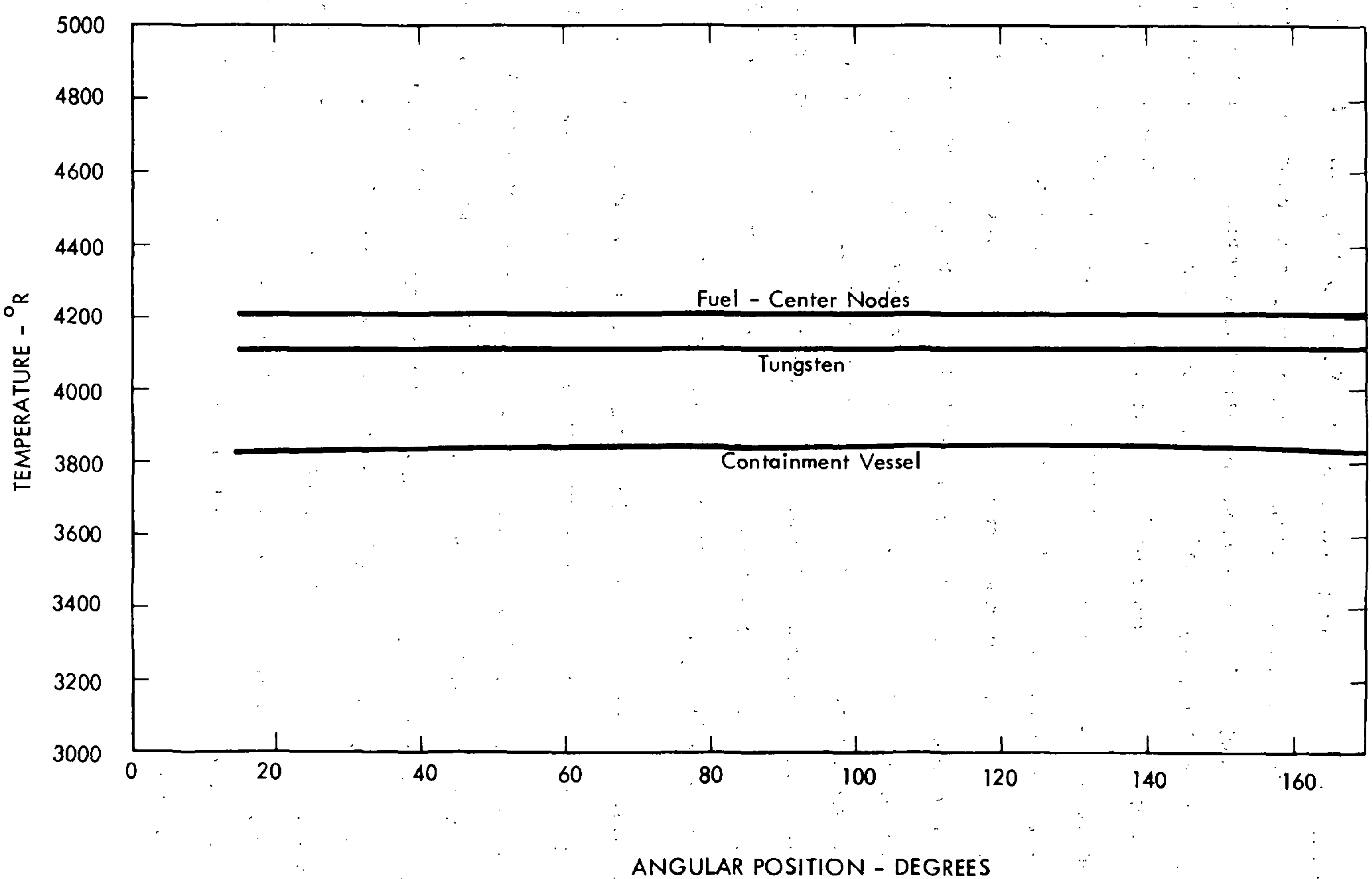

Figure 3-9. Circumferential Temperature Profile in System at Times = 2 Million Seconds (Case 2 Deep Burial)

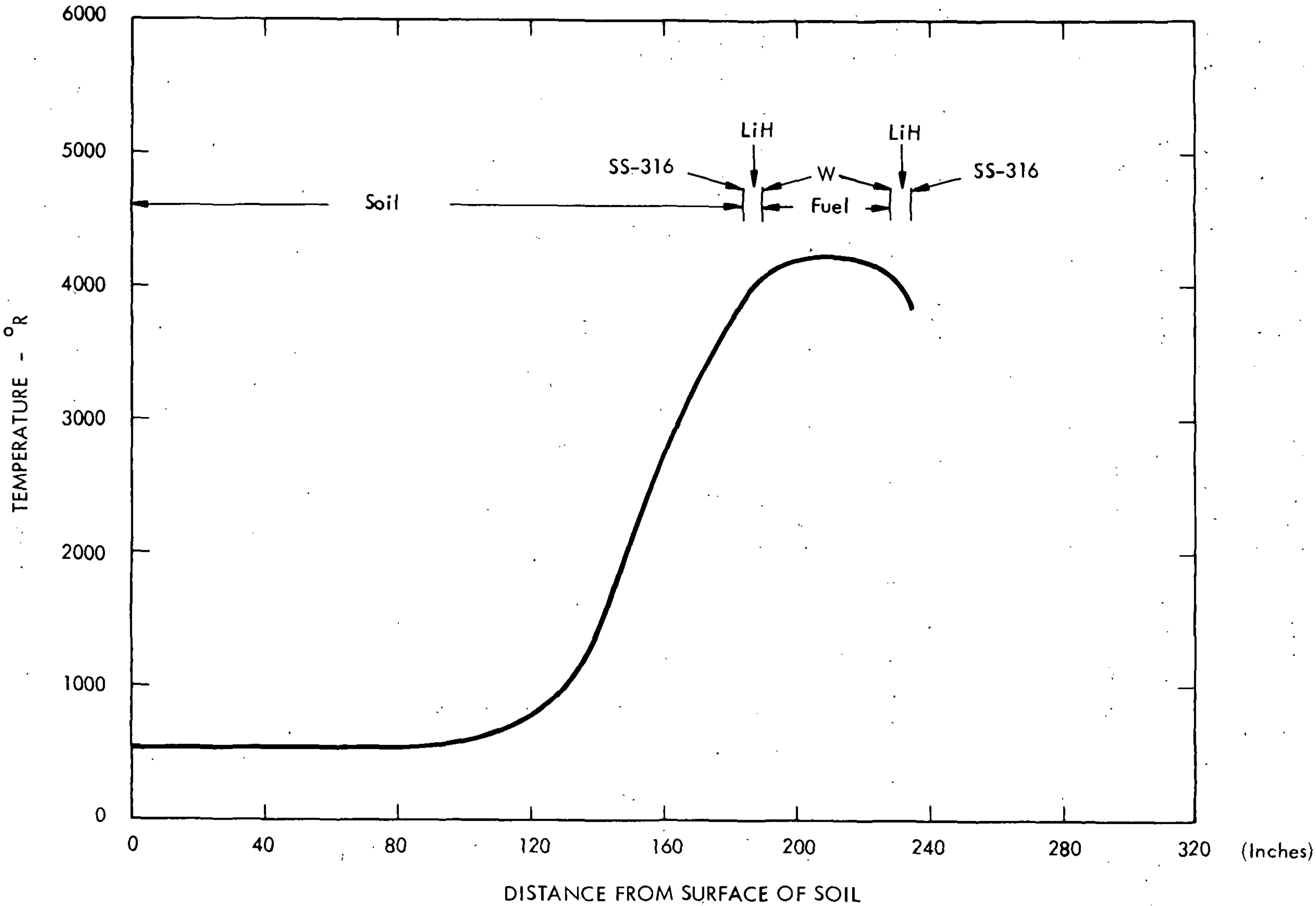

Figure 3-10. Centerline Temperature Profile from Surface to Base of Container (Case 2 - Deep Burial)
Time = 2 Million Seconds

The internal pressure response is shown in Figure 3-11. This response is shown for Case 2 with and without considering the effects of LiH dissociation. The effect of LiH dissociation is seen to be negligible for the first 200,000 seconds. At that point, the melting of LiH has been completed and the temperature level of the LiH is rising to levels such that a significant amount of dissociation is occurring to accelerate the internal pressure response. After 400,000 seconds, the containment vessel ruptured with a peak temperature of 2560°R and an internal pressure of 120 psi.

Figure 3-12 is a comparison of heat dissipation to the soil with the heat generation rate. Initially, the heat dissipation rate to the soil was 62 Btu/sec as compared to the 22.75 Btu/sec heat generation rate due to high initial reentry temperatures of the container. During the first 25,000 seconds the surface of the waste container and the soil in contact with the container converged in temperatures such that the heat flow rates converged. During the subsequent period to 200,000 seconds the container and soil temperatures started to rise due to the internal heat generation. Since part of the heat generated was being absorbed by the heating of the container, the heat dissipation rate dropped to a minimum of 4 Btu/sec. During the 200,000 to the 600,000 second period, the system was rising in temperature after all melting of the LiH was completed; however, the fraction of energy being absorbed was declining as indicated in the rise of the heat dissipation rate. After 1 million seconds, the temperatures and heat flow are seen to converge in Figure 3-12 as well as Figure 3-8.

3.3.3 Case 20 Results

Case 20 considered the deep burial of the solar escape module in podzol soil. This module was a 3 foot diameter waste container with a 7 K watts power level for the nuclear wastes, as shown in Tables 3-1 and 3-2. For this deep burial analysis the HTM-3 model in Figure 2-4 was used as with case 2. The nodes were assigned materials and radii indicated in Table 3-5.

Figure 3-13 shows the temperature response of the fuel center, tungsten, containment vessel and the soil one inch below the container axially from the center to the base of the container.

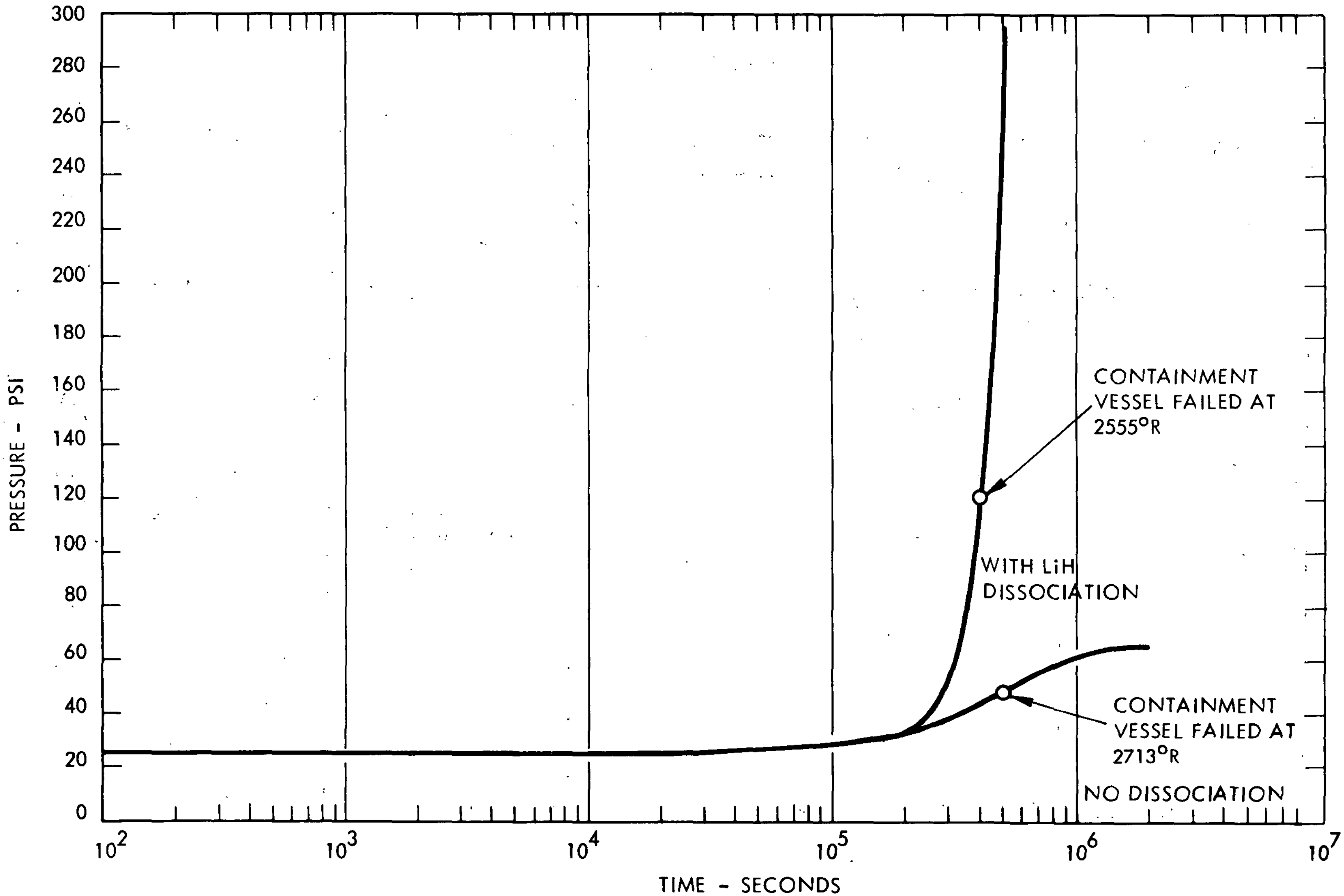

Figure 3-11. Internal Pressure Response for Case 2. (HTM-3)

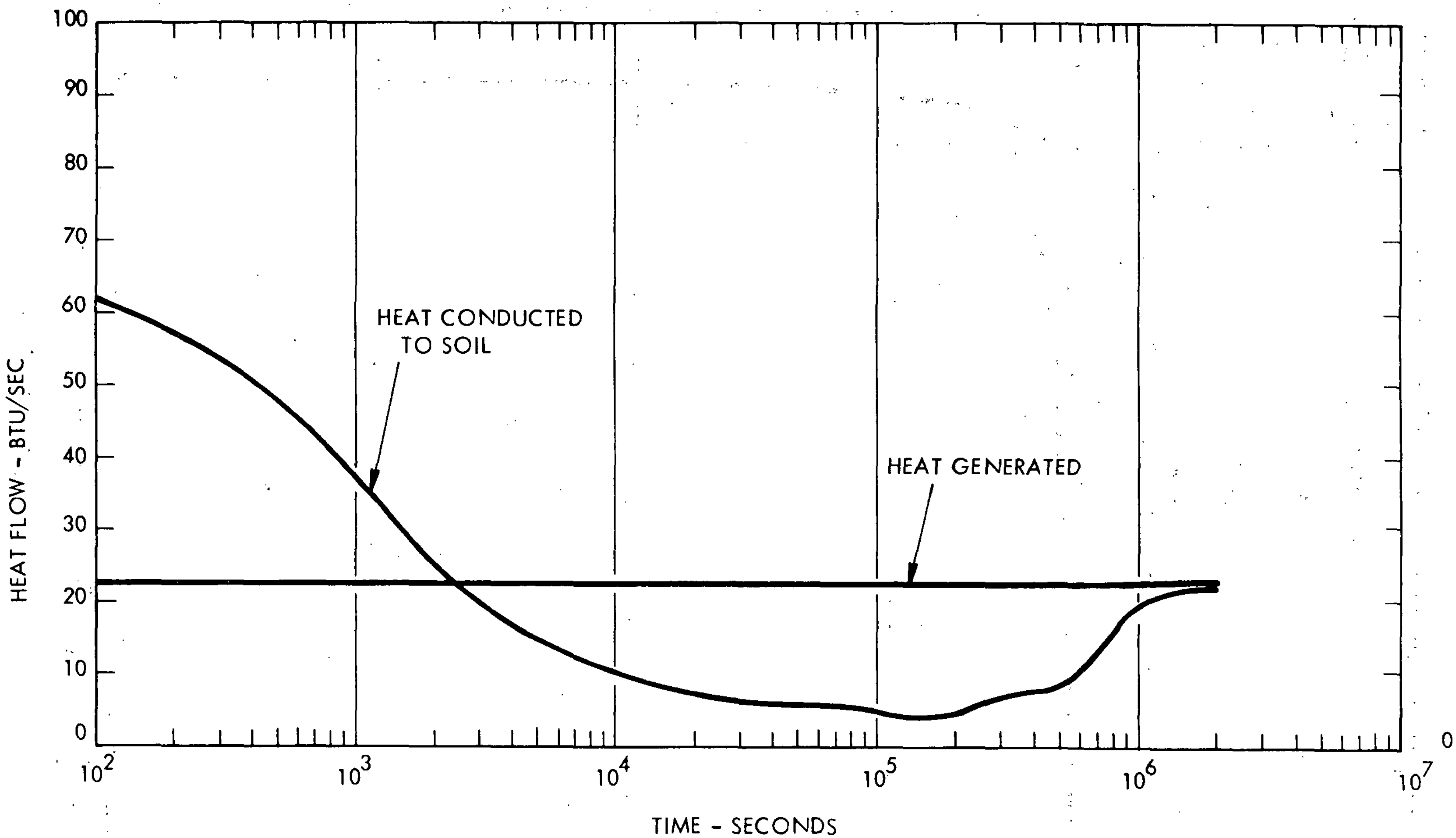

Figure 3-12. Heat Generation and Dissipation for Case 2

TABLE 3-5

CASE 20 RADII THICKNESSES AND MATERIALS

Deep Burial Model (Figure 2-4)

A. Spherical Section

Layer	Nodes	Outer Radius (Inches)	Material
1	109, 128, 146, 163, 180, 198	5.	Composite Fuel
2	110-199	11.27	Composite Fuel
3	111-200	12.67	Tungsten
4	112-201	14.	LiH
5	113-202	15.4	LiH
6	114-203	16.67	LiH
7	115-204	17.67	SS-316
8	116-205	18.67	Podzol
9	117-206	19.67	Podzol
10	118-207	20.67	Podzol

B. Upper Cylinder Section (All Coastal Plains Soil)

Row	Nodes	Thicknesses (In.)	Layer	Nodes	Outer Radii (In.)
1	1-9	32.	1	1, 10, 19, --, 100	10.34
2	10-18	32.	2	2, ---, 101	17.9
3	19-27	32.	3	3, ---, 102	20.67
4	28-36	32.	4	4, ---, 103	23.77
5	37-45	32.	5	5, ---, 104	30.90
6	46-54	32.	6	6, ---, 105	44.81
7	55-63	32.	7	7, ---, 106	71.69
8	64-72	32.	8	8, ---, 107	125.46
9	72-81	24.	9	9, ---, 108	238.38

TABLE 3-5 (Continued)

B. Upper Cylinder Section (All Coastal Plains Soil) - Continued

Row	Nodes	Thicknesses (In.)	Layer	Nodes	Outer Radii (In.)
10	82-90	20.			
11	91-99	16.			
12	100-108	6.			

C. Center Cylindrical Section (All Coastal Plains Soil)

Row	Nodes	Thicknesses (In.)	Layer	Nodes	Outer Radii (In.)
1	119-127	2.77	4	122, 140, ---, 211	23.77
2	138-145	7.37	5	123, ---, 212	30.9
3	156-162	10.34	6	124, ---, 213	44.81
4	173-179	10.34	7	125, ---, 214	71.69
5	190-197	7.57	8	126, ---, 215	125.46
6	208-216	2.77	9	127, ---, 216	238.38

D. Bottom Cylindrical Section (All Coastal Plains Soil)

1	217-225	3.1	1	217, 226, ---, 262	10.34
2	226-234	7.13	2	218, ---, 263	17.9
3	235-243	13.91	3	219, ---, 264	20.67
4	244-252	26.88	4	220, ---, 265	23.77
5	253-261	53.77	5	221, ---, 266	30.9
6	262-270	112.92	6	222, ---, 267	44.81
			7	223, ---, 268	71.69
			8	224, ---, 269	125.46
			9	225, ---, 270	238.38

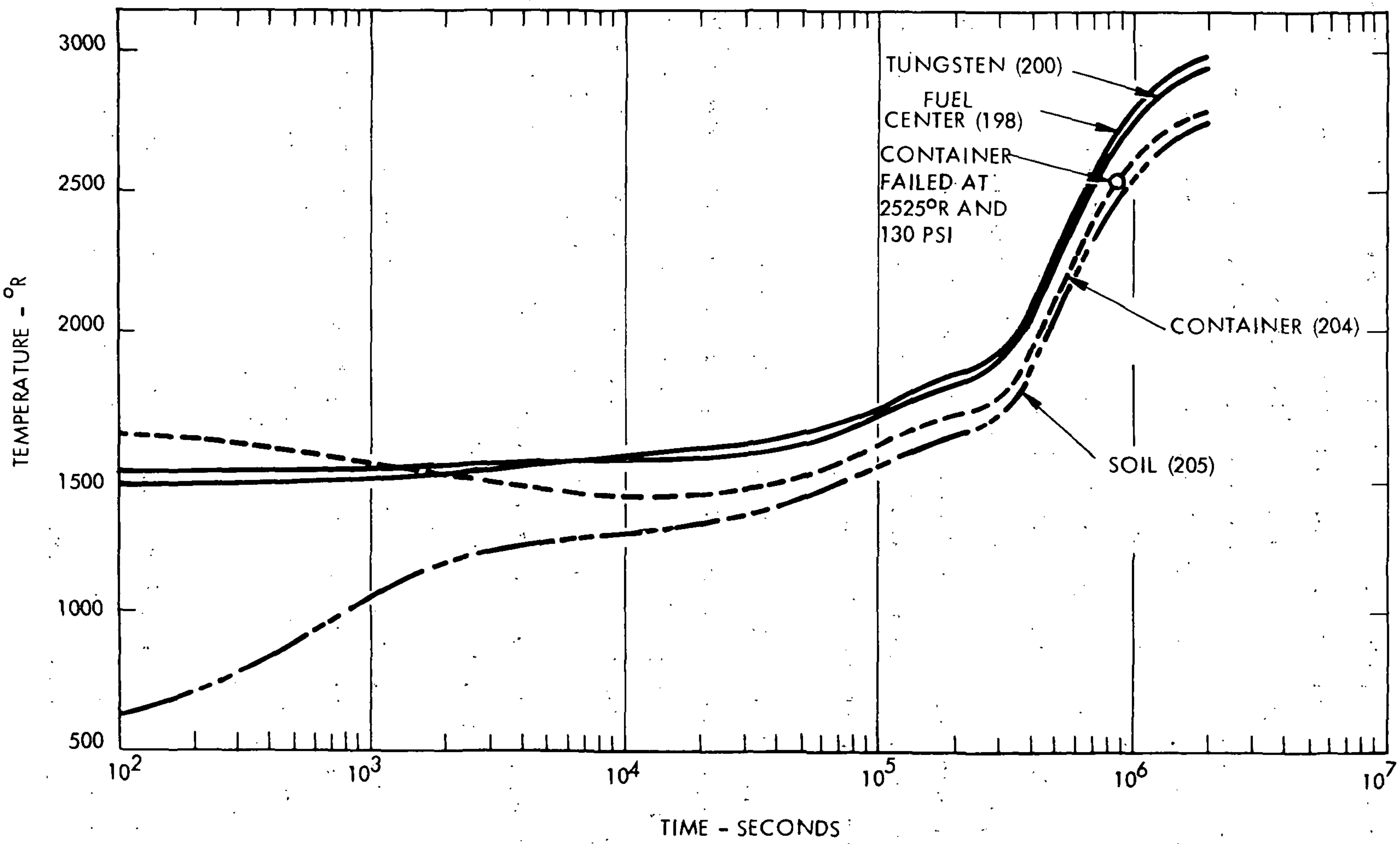

Figure 3-13. Axial Temperatures in Waste Container for Case 20

During the 2 million seconds that this case was run, the waste products rose to a level of 3000°R. As evidenced in the previous cases, the temperature gradient in the waste container was reversed during the initial period. Similar trends were observed for this transient as in case 2; however, the times for these trends to occur were longer due to the lower power level. For example, melting the LiH did not occur until 100,000 seconds versus approximately 30,000 seconds for case 2. Melting of the LiH was completed after 300,000 seconds versus 150,000 seconds for case 2. During the subsequent period, the system rose at a faster rate and dissociation of LiH occurred in sufficient quantity to increase the pressure response. A stress rupture failure occurred in the container after 870,000 seconds (10 days). At this point in time, the peak containment vessel temperature was 2500°R and the internal pressure was 130 psi. For case 2, failure occurred after 400,000 seconds (4.6 days); therefore, the lower power density package essentially doubled the containment lifetime after impact.

The circumferential temperature profile in the container was constant after 2 million seconds. This was the same trend as in case 2, indicating that the burial depth was sufficient that all heat flow was radial. Figure 3-14 is a plot of the model centerline temperature profile from the surface of the earth to the base of the waste container after 2 million seconds. No gradient was established in the soil over the first 20 feet of burial. As with case 2, the results indicate that burial depths of less than 10 feet would be required to influence the soil temperature response and potentially the container response.

The internal pressure response is shown in Figure 3-15. Essentially, no pressure response was indicated until after the LiH was molten and significant LiH dissociation had started which was 400,000 seconds after impact. During the subsequent period, the pressure response rose rapidly resulting in container rupture after 870,000 seconds.

Figure 3-16 is a comparison of heat dissipation to the soil with heat generation rate. Similar trends were observed for case 20 as with case 2. Temperatures and heat flow were essentially converged after 1.5 million seconds.

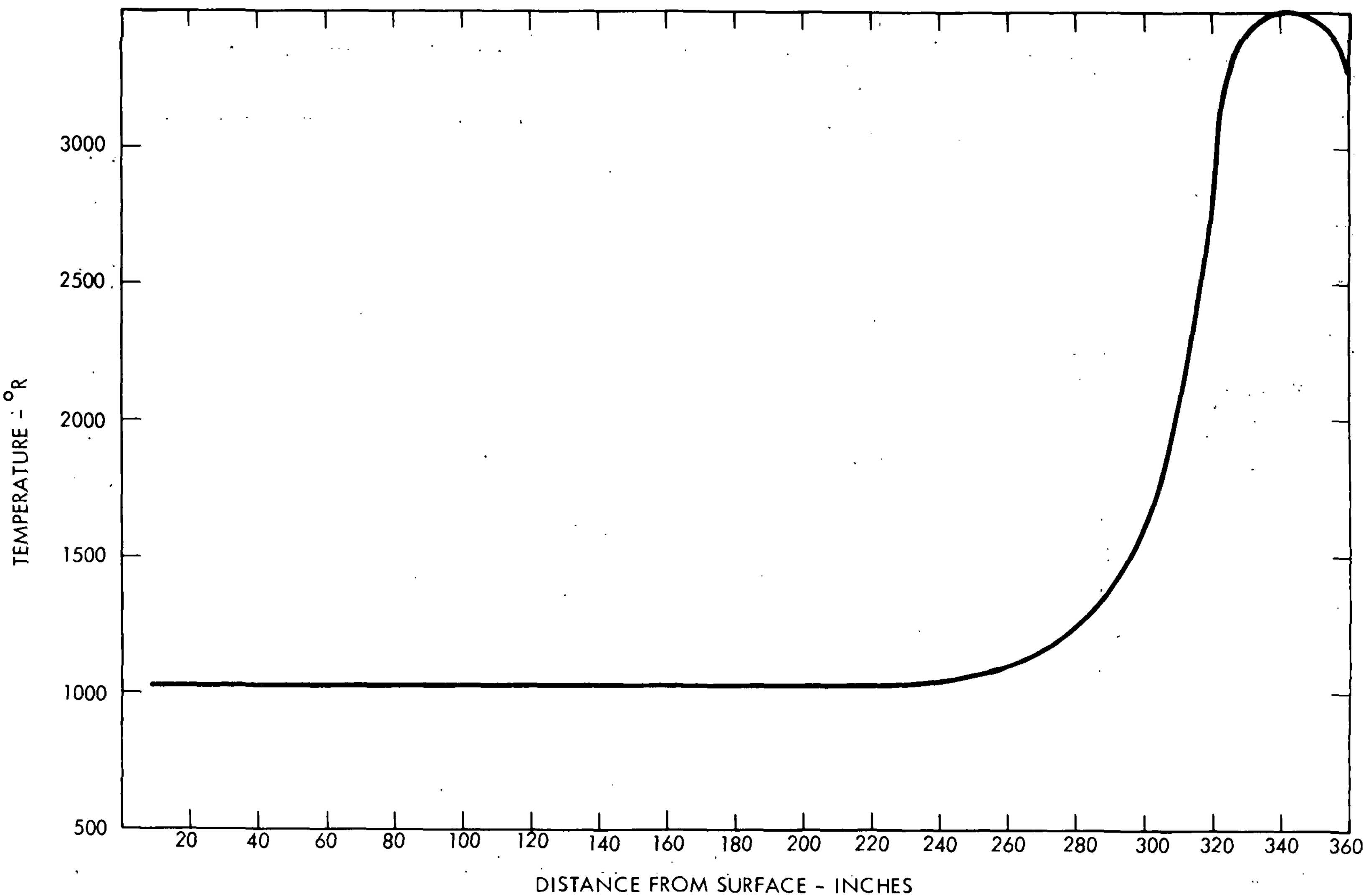

Figure 3-14. Centerline Temperature Profile from Surface of Soil to Base of Container (Time = 2 Million Seconds)

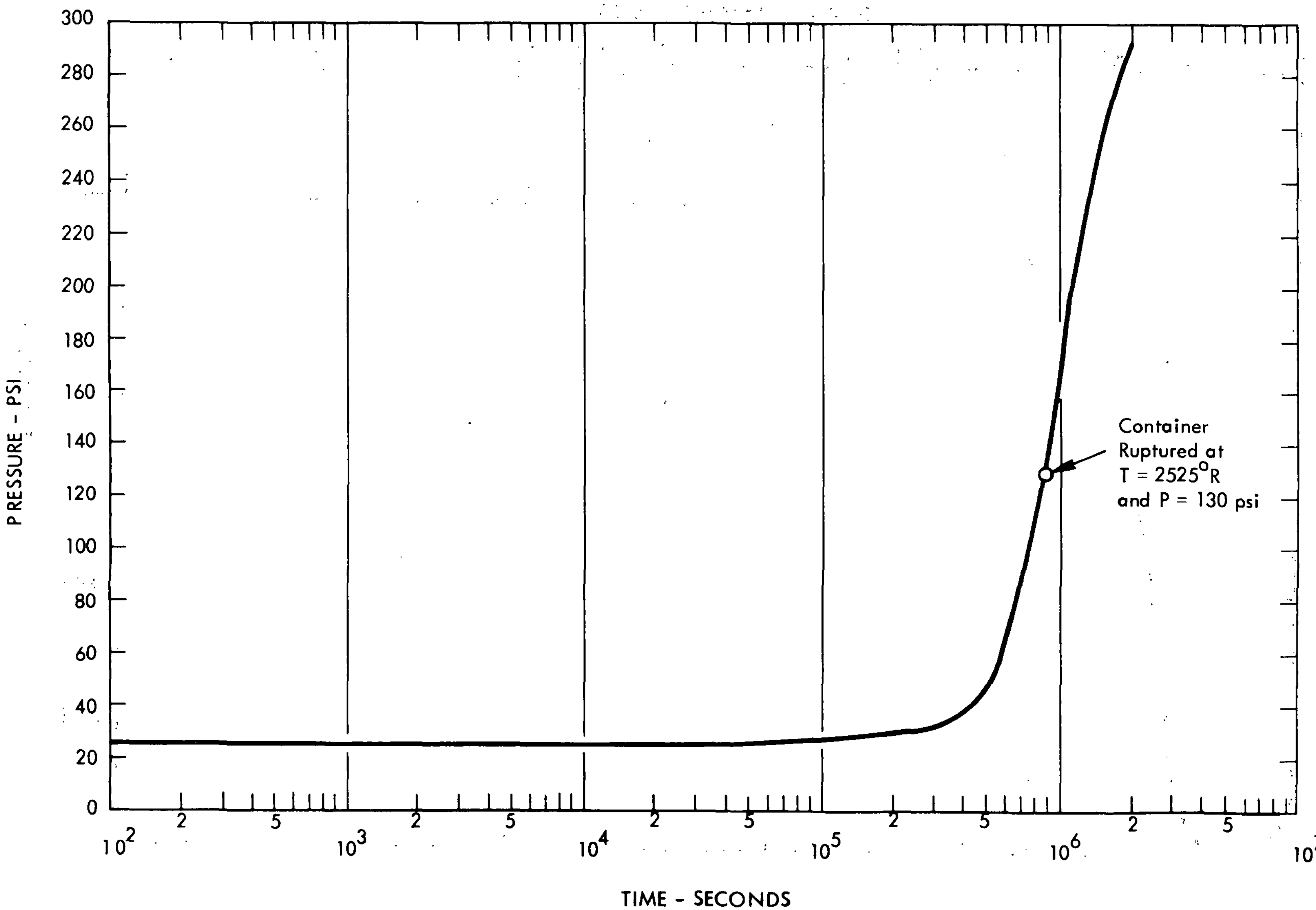

Figure 3-15. Internal Pressure Response for Case 20

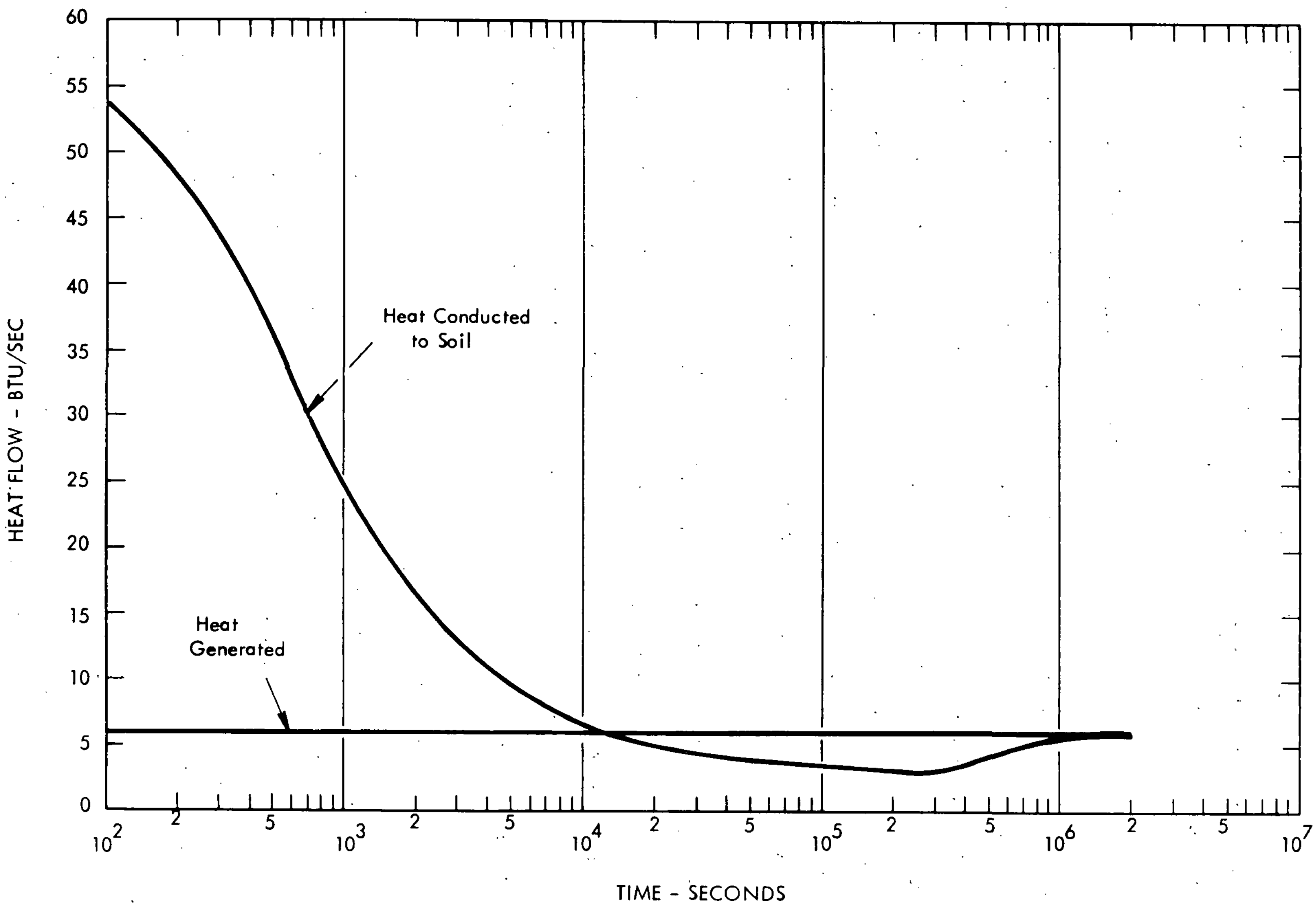

Figure 3-16. Heat Generation and Dissipation for Case 20

The results of case 20 were similar to case 2 with the notable conclusion that the container lifetime was doubled due to the combined effect of property variation and power level. Other comparisons described below are required to separate these effects.

3.4 PERTINENT DATA FROM 21 WASTE CONTAINER CONFIGURATIONS

For this study, analysis of the other 18 cases was limited to inspection and comparison of key results. For the purpose of these comparisons, Table 3-6 summarizes important assumptions and results. Assumptions in this table include the model, degree of burial, power level, container radius, waste material weight and soil material. Results shown in this table include maximum waste and container temperatures, approximate soil temperature, internal pressure, integrity of container and time that results are reported. If the container ruptured, the results are shown at the time of rupture. If no rupture occurred, the results are shown at the end of the transient.

3.4.1 Summary of HTM-1 Undeformed Container Results

Only one case was run for consideration of the undeformed configuration in a partial burial situation using the HTM-1 model. This case was case 1 described in Section 3.3.1. Key results were that internal temperatures and pressures dropped from initial levels due to sufficient exposure to air. The container integrity was maintained during the 23 day transient calculation.

3.4.2 Summary of HTM-2 Deformed Container Results

Cases 3, 8, 9 and 13 considered the waste container with significant deformation and in zero or partially buried situations. Case 3 considered the reference 4 foot diameter 24 K watt container with deformation of the container to the point of solidifying the void areas in the base of the container. Zero burial (resting on top of ground) was assumed. Due also to sufficient air exposure, the temperature levels in the container dropped to levels of $1300^{o}R$ in the waste material and $900-1200^{o}R$ in the container. The internal pressure dropped also and the container remained intact based on the premise that the container was intact initially after impact.
Case 13 also considered the 24 K watt reference waste container but with approximately 25% burial in coastal plains soil. With 25% burial, the temperature levels dropped in the container

TABLE 3-6

SUMMARY OF HEAT TRANSFER CALCULATIONS

CASE NUMBER	1	2	3	4	5	6	7	8	9	10	11	12	13	14	15	16	17	18	19	20	21
MODEL	Un Def	DB	Def.	DB	DB	DB	DB	Def.	Def.	DB	DB	DB	Def.	DB	DB	DB	DB	DB	DB	DB	DB
Degree of Burial	37.5%	19'	0	22'	30'	30'	30'	0	25%	33'	33'	33'	25%	33'	6'	9'	14'	22'	30'	30'	30'
Power, Kw	24	24	24	1.5	5	7	10	7	7	15	20	30	24	24	24	24	24	1.5	5	7	10
C. V. Radius, In.	25.3	25.3	25.3	12	15.4	17.7	17.7	17.7	17.7	25.3	25.3	25.3	25.3	25.3	25.3	25.3	25.3	12.0	15.4	17.7	17.7
Weight (Waste), Lb.	800	800	800	50	167	233	300	233	233	500	666	900	800	800	800	800	800	50	167	233	300
Max. Waste Temp., °R	1478	2750	1309	2147	2770	2760	2785	1016	1049	2710	2720	2730	1396	2800	2850	2850	2850	1750	2680	2700	2850
Max. C. V. Temp., °R Bottom	1417	2555	1236	2111	2575	2560	2574	984	1017	2499	2514	2532	1342	2550	2600	2600	2600	1700	2525	2525	2550
Top	985		933					834	849				960		2575	2575	2575	1700	2525	2525	2550
Soil Temp. at 2 Ft., °R	650	600	650	800	600	650	600	590	600	600	600	600	700	650	650	650	650	700	700	700	650
Internal Pressure, Psi	21	120	18	43	131	129	125	15	15	109	111	108	19	133	135	133	133	28	122	131	140
C. V. Failure	No	Yes	No	No	Yes	Yes	Yes	No	No	Yes	Yes	Yes	No	Yes	Yes	Yes	Yes	No	Yes	Yes	Yes
Time, Days	23	4.5	23	23	7	6.7	4.3	23	23	7.7	5.5	3.6	23	5.4	5.4	5.4	5.4	23.4	12.2	10	5.4
Soil	Coastal Plains													Podzol							

NOTE: Temperatures and Pressures are at the Indicated Times to levels approximately 100°R higher than for zero burial. The integrity of the container was maintained.

Cases 8 and 9 considered the solar escape module in a deformed configuration with zero and 25% burial also. Both cases dropped to levels of 1000°R in the waste material and 800-1000 in the container. The internal pressure dropped to 15 psi. Both cases survived the 23 day transient. For the solar escape modules, zero versus 25% burial resulted in 15-35°R variations in container temperatures.

3.4.3 Summary of HTM-3 Deep Burial Container Results

The remaining 16 cases considered the deep burial of various containers with the HTM-3 model utilized. All cases resulted in significant increases in container temperatures ultimately resulting in container stress rupture except for the low power (1.5 K watt) solar escape module. For the cases considered, time to failure ranged from 3.6 days for a 30 K watt container buried in coastal plains soil to 12.2 days for a 5 K watt solar escape module buried in podzol. Container temperatures were approximately 2500-2600°R and internal pressures were approximately 110-140 psi at the time that rupture occurred for all the cases. The 1.5 K watt powered containers (cases 4 and 18) reached a level of 2100°R in coastal plains soil and 1700°R in podzol. Internal pressures were 40 and 30 psi respectively for burial in coastal plains soil and podzol soil.

3.5 DISCUSSION OF RESULTS

Referring to Table 3-6, several comparisons were made between cases.

3.5.1 Effect of Impact Conditions on 24 K watt Reference Design

Cases 1, 2, 3 and 13 were analyses of the 24 K watt reference container impacting coastal plains soil with and without deformation. Cases 1 and 2 provided a comparison of partial burial of an undeformed container to deep burial. Whereas for the partial burial case (37.5% burial), the temperature level dropped to sufficiently low levels to insure safe containment, a deep burial (19 feet) resulted in significant heating causing a rise in internal pressure and ultimately a creep rupture failure after 4.5 days. Case 3 considered a deformed container sitting on the surface of the ground. This case resulted in the temperature levels in the container of approximately 180°R lower than case 1 (1420°R for case 3 versus 1340°R for case 1 for the maximum container temperature). As with case 1, the container remained intact during the transient. The lower temperatures were achieved because of the greater surface area of the deformed container exposed to air. A comparison of case 13 (deformed container with 25% burial) to case 3 indicated an increase in container temperatures of approximately 90°R for the partially buried case 13; however, the container remained intact.

3.5.2 Comparison of Alternate Container Designs Buried in Coastal Plains Soil

Cases 4-7 considered four alternate waste container designs ranging in power from 1.5 to 10 K watts and ranging in outer radius from 12 to 18 inches. These cases considered deep burial in coastal plains soil. The low power module (1.5 K watts in a 12 inch outer radius) reached a container temperature level of 2100°R and an internal pressure of 40 psi after 23 days. At these conditions, the integrity of the container was maintained. Cases 5, 6 and 7, which considered modules with 5, 7 and 10 K watts of nuclear wasts, rose to sufficient temperature and pressure levels to result in container stress rupture. Obviously, the time to rupture varied inversely with the power level (7, 6.7 and 4.3 days from impact to rupture versus 5, 7 and 10 K watts). The limited variation in geometry and capacitance of the container was secondary to the changes in power level in terms of their effect on response time. Comparison of cases 7 and 2 indicated that the higher powered 24 K watt container with the larger capacitance of a 25 inch radius container resulted in the same time to rupture (4.5 days versus 4.3 days) as the lower powered 10 K watt module enclosed in a lighter 18 inch radius container. Thus, higher power levels can be achieved at the expense of additional thermal capacitance and, thus, weight.

3.5.3 Effect of Deformation and Partial Burial on Solar Escape Module

Cases 6, 8 and 9 provided a comparison of container deformation for the 7 K watt solar escape module. Case 8 assumed the container to be deformed and setting on top the ground. Case 9 considered a 25% burial of the deformed container. Due to the exposure to air, cases 8 and 9 reached low values of peak container temperatures (98°R and 1020°R, respectively) such that rupture of the container did not occur. A hard impact with only partially burial is less severe in thermal response effects than burial in soft soil if the container survives impact.

3.5.4 Effect of Power Variation in 25 Inch Radius Container

Cases 2, 10, 11 and 12 provided a comparison of the effects of power level on containers of approximately the same capacitance. All four cases considered the container as deeply buried and all four cases resulted in a stress rupture of the container due to excessive temperatures and pressures. The 15 K watt container survived 7.7 days before a rupture occurred. The 20, 24 and 30 K watt containers failed after 5.5, 4.5 and 3.6 days respectively. A comparison of cases 5 and 10 indicated that approximately the same container lifetime for 15 K watts of nuclear material in a 25 inch container as for 5 K watts of power in a 15 inch container.

3.5.5 Comparison of Soil Property Variation for the 24 K Watt Container

Cases 14-17 considered burial depths varying from 6 feet to the base of the container to 33 feet to the base of the container for the 24 K watt 4 foot diameter containers. All 4 cases failed at the same point in time (5.4 days in podzol soil). For the shallow burial of 6 feet, the surface rose to a maximum of 70°F above ambient at the time of failure. The combined heat transfer coefficient for convection and radiation at the surface was approximately 1.5 Btu/hr-ft^2-°R. The heat loss from the surface, therefore, did not significantly alter the response of the waste container. A moderately shallow burial, therefore, still resulted in a container rupture.

3.5.6 Comparison of Burial Depth for the 24 Kwatt Container

Cases 14-17 considered burial depths varying from 6 feet to the base of the container to 33 feet to the base of the container for the 24 K watt, 4 foot diameter containers. All four cases failed at the same point in time (5.4 days in podzol soil). For the shallow burial of 6 feet, the surface rose to a maximum of 70°F above ambient at the time of failure. The combined heat transfer coefficient for convection and radiation at the surface was approximately 1.5 Btu/hr-ft^2-°R. The heat loss from the surface, therefore, did not significantly alter the response of the waste container. A moderately shallow burial, therefore, still resulted in a container rupture.

3.5.7 Comparison of Soil Property Variation for Alternate Waste Container Configurations

Cases 18-21 were repeats of cases 4-7 with the soil changed from coastal plains soil to podzol soil. Comparison of cases 4 and 18 indicated that the container reached a level of 1700°R for deep burial in podzol which was 400°R lower than for burial in coastal plains soil. Both 5 KW containers resulted in a stress rupture failure; however, the post impact lifetime was increased by 75%. For the 7 KW and 10 KW system, the increase in lifetime was 50% and 20% respectively. The effect of burial in a more conductive soil; therefore, was an increase in the lifetime; however, the improvement dropped with increase in power level.

3.5.8 General Discussion

For those cases of deep buried containers where rupture occurred, the container temperature and internal pressure levels were 2550°R and 130 psi respectively. The rise in temperature induced the rise in pressure due to the dissociation of LiH. For the higher powered systems, the ultimate temperature level of the container was 3000-3500°R due to the soil characteristics. In fact, the melting point of coastal plains soil is reported at 3400°R and for podzol soil is 3000°R. In these cases, the heat of fusion and change in soil conductance could not be utilized to flatten the response of the container prior to stress rupture. To fully utilize the soil property changes requires raising the temperature level capability of the container. One means of accomplishing this is to consider alternate container materials. Another means is to relieve the internal pressure response. Potential mechanisms for performing the latter function are venting of the gas and providing a getter for the hydrogen released from the LiH. These pressure relieving devices were not considered in the present study.

Another area of consideration is the adequacy of the soil properties. The thermal conductance of common soils have been extensively and accurately defined (Reference 5, for example); however, data is lacking or specific heat and heats of fusion. The adequacy of the present analysis in describing the response of the container and soil at temperatures above 2500°R might, therefore, be questionable to a degree.

4.0 CONCLUSIONS

As part of this program, the ESATA computer program was successfully adapted to the problem of analyzing the post impact thermal behavior of partially and deep buried radioactive nuclear waste material containers. A general type of container consisting of spherical layers of waste material tungsten shielding, LiH shielding and SS-316 container wall was considered in this analysis. Twenty-one cases were studied which included variations in container geometry, power level, degree of deformation, degree of burial and soil properties. Three of the cases were analyzed in detail and the remaining 18 were compared for overall results. Conclusions obtained from this study are:

1. Zero and partial burial (up to 37.5% diametral) of undeformed and deformed containers resulted in a decline in container temperature from a 1660°R initial level induced by renetry heating to 1000-1400°R levels.

2. The container integrity was maintained (assuming no rupture due to impact) for the zero and partial burial of the undeformed and deformed containers for the 23 day transients (2 million seconds).

3. The deep burial (in excess of 10 feet) of the 24 KW, 2 foot radius waste containers resulted in container temperatures in excess of 3000°R for both coastal plains soil and podzol soil.

4. The deep burial of all waste container designs considered with 5 KW or more of power (5 KW to 30 KW in containers of 12 inch to 25 inch outer radii) resulted in stress rupture of the container. The post impact lifetime of these containers varied from 3.6 days for a 30 KW, 25 inch radius container to 12.2 days for a 5 KW, 15 inch radius container.

5. The 15 KW, 12 inch radius containers stabilized at sufficiently low temperatures to insure the integrity of the container for the transient period analyzed of 23 days.

6. For those cases in which stress rupture occurred, the container temperature level was 2500-2600°R and the internal pressure was 120-130 psi.

7. The main component to the pressure response was hydrogen released from LiH dissociation.

8. The container temperature level at rupture was less than the estimated melting point of the soils considered.

9. Variation in burial depths from the soil surface to the base of the containers of 6 feet to 30 feet did not significantly affect the container temperature response.

10. Soil surface temperatures were at ambient temperature for deep burial cases and rose to 70°R above ambient for burial depths as small as 6 feet.

11. Consideration of the better conducting podzol soil increased the container post impact rupture lifetime by 20-75% dependent on power level.

5.0 REFERENCES

1. Plan for the Management of AEC-Generated Radioactive Waste, United States Atomic Energy Commission, WASH-1202, January 1972.

2. Parker, W. G., VanBibber, L. E. and Tang, Y. S., Final Report - Afterheat Distribution of a Mobile Nuclear Power Plant, NASA CR-120825, Westinghouse Astronuclear Laboratory, November 1971.

3. Parker, W. G., VanBibber, L. E., et. al., Final Report - Reactor Safety Study for Nuclear Powered Aircraft, Westinghouse Astronuclear Laboratory, Contract F29601-72-C-0035, February 1973.

4. Pierce, B. L. and Stumpf, H. J., TAP-A - A Program for Computing Transient or Steady State Temperature Distributions, Westinghouse Astronuclear Laboratory, WANL-TME-1872, December 1969.

5. Flynn, D. R. and Watson, T. W., Measurements of the Thermal Conductivities of Soils to High Temperatures - Final Report, National Bureau of Standards (Sandia Laboratories), SC-CR-69-3059, April 1969.

APPENDIX A

OPERATING INSTRUCTIONS
FOR THE ESATA CODE

A. 1 INPUT DATA

The quantity of input data required for the operation of any computer program becomes particularly important whenever the program is to be employed for analysis of many different configurations. To be effective in performing safety analysis of various post impacted nuclear waste disposal container configurations, the analysis tool must be easy to use and the input data minimized. For this reason, generalized heat transfer models were developed for the ESATA program in order to minimize the input data required and thus maximize the usefulness of the program.

The general types of input data required are as follows:

- Variable array size for geometry related parameters.
- Title
- Initial and final times for the calculation, time increment and convergence criteria.
- Set of numbers to identify model choice, degree of burial, soil selection and temperature, soil-to-containment system interface condition, total heat generation rate, soil fusion temperature, amount of emitting fuel and containment system void fraction.
- Outer radius, material and initial temperature for each spherical layer.
- For deformed model, thickness of each layer in deformed base.
- For deep burial model, thickness of each soil layer above spherical portion of model.
- The time during the transient period where output data is required.
- The times during transient when all data in common blocks are placed on the restart tape.

The specific input data required by the user in order to operate the afterheat temperature analysis option of the ESATA program is given in Table A-1.

The ESATA program contains specific heat transfer models, as previously mentioned, to minimize input data requirements. However, since the ESATA program was formed from the TAP-A program, the general TAP-A input data options can be used to "override" or "modify" certain features of the HTM's contained in ESATA. The following types of modifications are possible using the standard TAP-A input data options.

- Initial temperature distribution (as opposed to uniform component temperatures) for the power plant configurations can be input.
- Node volumes (thickness) and materials can be varied.
- Boundary conditions can be varied.

A.2 OUTPUT DATA

Computer output from an ESATA program calculation consists of an edit of the input data, the results from translation of the input data into the nodal point form required for the finite difference solution, and the data output from the calculations. The following units apply to all the output data:

Temperature - ^{o}F
Heat Flow - Btu/sec
Heat Flux - Btu/sec-in^2
Power - Btu/sec
Film Coefficients - Btu/sec-in^2
Conductivities - Btu/sec-in-^{o}R
Specific Heat - Btu/lb-^{o}R
Volumes - in^3
Area - in^2
Admittances - Btu/sec-^{o}R
Weights - pounds

TABLE A-1 - ESATA INPUT DATA FOR ANALYSIS OF FISSION PRODUCTS WASTE DISPOSAL BURIAL ANALYSIS

Note: Specific values are indicated for those parameters that can remain fixed the majority of the computations.

CARD NO.	COLUMNS	FORMAT	FORTRAN SYMBOL	DESCRIPTION	VALUE	UNITS
1	1-5	I5	MAXINT	Number of Internal Nodes	300	Dimensionless
	6-10	I5	MAXSUR	Number of Surface Nodes	42	Dimensionless
	11-15	I5	MAXBND	Number of Boundary Nodes	5	Dimensionless
	16-20	I5	MAXCON	Number of Internal Connectors Per Node	6	Dimensionless
	21-25	I5	MAXRAD	Number of Surface Nodes Connected to a Boundary Node	5	Dimensionless
	26-30	I5	MAXTAB	Number of Boundary Temperature Tables	5	Dimensionless
	31-35	I5	MTABEN	Number of Boundary Table Entries	5	Dimensionless
	36-40	I5	MAXQQ	Number of Power Table Entries	5	Dimensionless
	41-45	I5	MAXPRT	Number of Print Out Times	50	Dimensionless
	46-50	I5	MAXFIL	Number of Film Coefficient Tables	5	Dimensionless
	51-55	I5	MFILEN	Number of Film Coefficient Table Entries	5	Dimensionless
	56-60	I5	IMAXAV	Number of Averages	5	Dimensionless
	61-65	I5	MAXTYP	Number of Types of Connectors	5	Dimensionless
2	1-2	I2	ISATA	Trigger for Selecting Calculation Option	0 for general heat transfer analysis. 1 for afterheat temperature analysis. n (n>1) for restarting an afterheat temperature analysis where n-1 indicates the restart case selected.	
	3-58	14A4	ID	Problem Tite		
3	1-10	F10.0	TIMEO	Initial Time	0	Seconds
	11-20	F10.0	TIMFIN	Final Time		Seconds
	21-30	F10.0	DELTAT	Time Increment	60	Seconds
	31-40	F10.0	CRIT	Convergence Criteria on Heat Balance	0.05	Dimensionless
	41-50	F10.0	Z (2)	Problem Type (Transient or Steady State)	3	Dimensionless
	51-60	F10.0	Z (1)	Number of Iterations Before a Second Order Extrapolation on Temperature is Made	50	Dimensionless
	61-70	F10.0	ERFC	Maximum Number of Iterations (If this value is exceeded during any one time increment, problem will be terminated)	2000	Dimensionless
	71-80	F10.0	DELTT	Temperature Increment for Calculation of Effective Specific Heat to Simulate Heat of Fusion. If DELTT = 0.0 via input, DELTT = 50	50	°R
4	1-5	I5	IMODEL	Model Configuration Option	1 for undeformed model 2 for deformed model 3 for deep burial model	Dimensionless

Astronuclear Laboratory

CARD NO.	COLUMNS	FORMAT	FORTRAN SYMBOL	DESCRIPTION	VALUE	UNITS
	6-10	I5	IBURY	Degree of Soil Burial Option (number of nodes circumferentially exposed to air)	0-8 (0-6 for IMODEL = 3)	Dimensionless
	11-15	I5	MATSOL	Material Number for Soil Nodes		Dimensionless
	16-20	I5	NCONT	Spherical Layer Number Representing Containment Vessel		Dimensionless
	21-25	*I5*	*NSURF*	*Spherical Layer Number Representing Outer Shell of Waste Disposal System*		*Dimensionless*
	26-30	I5	MATCOR	Material Number of System Heat Sources		Dimensionless
	31-35	I5	LOGIC	Trigger for Printout of Detailed Node Generator Data =	0 or 1 - None > 1 - Detailed Prints	Dimensionless
5	1-10	F10.3	TEMSOL	Initial Soil Temperature		^oR
	11-20	F10.3	TAMB	Initial Air Temperature		^oR
	21-30	F10.3	CCOEF	Contact Coefficient for Containment/Soil Interface	< 0 radiation (-EF) = 0 soil properties > 0 contacts coefficient	Dimensionless Dimensionless Btu/hr-ft^2 ^oR
	31-40	F10.3	QTOT	Total Heat Generation Rate		Btu/sec
	41-50	F10.3	TFUSE	Soil Fusion Temperature		^oR
	51-60	F10.3	CSVOID	Containment System Void Fraction		Dimensionless
	61-70	F10.3	PTOT	Internal Pressure		Psi
6	1-10	F10.3	RO(I)	Outer Radius of I th Spherical Layer		Inches
	11-15	I5	LAYMAT(I)	Material Number for I th Spherical Layer		Dimensionless
	16-25	F10.3	TEMLAY(I)	Initial Temperature for I th Spherical Layer		^oR
			Repeat set of 3 variables for I + 1 and I + 2 layers in columns 26-50 and 51-75 respectively. Repeat card 5 to define the first through NSURF th layer.			
7	1-10	F10.3	WEIGHT (1)	Weight of Waste Products in Core		Lbs.
	11-20	F10.3	WEIGHT (2)	Weight of Aluminum in Core		Lbs.
	21-30	F10.3	WEIGHT (3)	Weight of LiH in Core		Lbs.
	31-40	F10.3	WEIGHT (4)	Weight of Copper in Core		Lbs.
8			*This card is for deformed model only (IMODEL = 2). Ignore otherwise.*			
	1-80	8F10.3	THC(I)	I = 15, 28 Thickness of rows of nodes in deformed base	THC (15) - Nodes 5, 23, etc. THC (16) - Nodes 6, 24, etc.	Inches
9			This card is for deep burial model only. (IMODEL = 3) Ignore otherwise.			
	1-80	8F10.3	THC(I)	I = 11, 22 Thickness of Rows of Nodes in Top of Model	THC (11) - Nodes 1, 2, 3, etc. THC (12) - Nodes 10, 11, 12, etc.	Inches
10A-10N	1-2	I2	IG	Card Type Identifier	11	Dimensionless
	3-7	F5.0	AO	Table Entry Position		Dimensionless
	8-12			Blank		
	13-73	6E10.0	Z(K) K = 2, 7	Times for output data to be printed. Six printout *times can be included on each card; the number of cards A-N is dependent on the number of printout times requested.*		Seconds

CARD NO.	COLUMNS	FORMAT	FORTRAN SYMBOL	DESCRIPTION	VALUE	UNITS
11A-11N	1-2	I2	IG	*Card Type Identifier* Remainder of card similar to card 9. *Times for common blocks to be stored on auxiliary tape for restarting.*	16	
N	Normal TAP-A input data cards are inserted here and will override the HTM data contained in ESATA.					
N + 1	1-2	I2	IG	Trigger to end data input for a single card	25	Dimensionless
N + 2	1-2	I2	ISATA	Trigger to indicate that no more cases are to be run	99	

ESATA INPUT DATA FOR RESTART OF A CASE

CARD NO.	COLUMNS	FORMAT	FORTRAN SYMBOL	DESCRIPTION	VALUE	UNITS
1	1-5	I5	MAXINT	Number of Internal Nodes	360-720	dimensionless
	6-10	I5	MAXSUR	Number of Surface Nodes	55	dimensionless
	11-15	I5	MAXBND	Number of Boundary Nodes	5	dimensionless
	16-20	I5	MAXCON	Number of Internal Connectors Per Node	6	dimensionless
	21-25	I5	MAXRAD	Number of Surface Nodes Connected to a Boundary Node	5	dimensionless
	26-30	I5	MAXTAB	Number of Boundary Temperature Tables	5	dimensionless
	31-35	I5	MTABEN	Number of Boundary Table Entries	5	dimensionless
	36-40	I5	MAXQQ	Number of Power Table Entries	5	dimensionless
	41-45	I5	MAXPRT	Number of Print Out Times	50	dimensionless
	46-50	I5	MAXFIL	Number of Film Coefficient Table	5	dimensionless
	51-55	I5	MFILEN	Number of Film Coefficient Table Entries	5	dimensionless
	56-60	I5	IMAXAV	Number of Averages	5	dimensionless
	61-65	I5	MAXTYP	Number of Types of Connectors	5	dimensionless
	(A Minimum Value of 1 is Required for Each Variable)					
2	1-2	I2	ISATA	Trigger for Selecting Calculation Option	N (n 1) where N-1 indicates the restart case selected	dimensionless
	3-58	14A4	ID	Problem Title		dimensionless
3	1-10	E10.0	TIMFIN	Final Time for Transient		seconds
	11-15	I5	NCCL	Maximum Number of Iterations (If =0 Value Unchanged from Previous Case)		dimensionless
	16-25	E10.0	DELRTT	Increment Between Restart Tape Usage in Cp Time (If -0 Value Unchanged from Previous Case)		
N	Normal TAP-A Input Data, Including Printout Times can be Inserted here.					
N-1	1-2	I2	IG	TRIGGER to End Data Input for a Single Case	25	dimensionless
N-2	1-2	I2	ISATA	TRIGGER to Indicate that No More Cases are to be Run	99	dimensionless

Time - seconds

Dimensions - inch

Pressure - psi

Stress - psi

The following sections describe in detail each form of output:

A.2.1 Input Data Edit

The first part of the printed output is an edit of the input data. The following quantities are printed out in the sequence indicated.

1) Computer storage requirements for the problem. (Summary output of Card 1 of the input data.)

2) The decimal starting locations of all variable size matrices in the program.

3) The problem title (defined by Card 2 of the input data).

4) An identification of the model type to be analyzed and initial container and environment conditions. (Card 4 in the input data)

5) Spherical layer input data including initial temperatures, inner radii and material numbers. (Card 5 in the input data.)

6) List of material number designations including weights of fuel components. (Card 6 in the input data.)

7) For deformed model, the compacted layer input including initial temperature, thickness and material number or for deep burial shell and layer dimensions. (Cards 7 and 8 in the input data.)

8) Initial core temperature, environmental temperatures and internal pressure.

9) A reproduction of any of the standard TAP-A input cards including cards identifying printout times. (Card 16A through 16N and the N cards of the input data.)

A.2.2 Translation of Input Data

The next portion of the output data consists of the results from the translation of the input data into the nodal point form required for finite difference solution. The following data are printed out in the sequence indicated:

1) The problem title (as defined by Card 2 of the input data).

2) Initial and final times for the problem including the initial time increment and the convergence criteria (as defined by Card 3 of the input data).

3) If applicable, a listing of the boundary temperature tables.

4) If materials are identified which are not contained in the program, then property data for these materials are output.

5) A matrix identifying for each node, the volume, heat generation rate, initial temperature and capacitance.

6) A matrix identifying the admittances and neighboring nodes for each node in the model.

7) If a table of film coefficients is output, if different than those contained in the program.

8) A matrix of surface to boundary node connectors including initial temperatures, heat transfer mechanism, surface area, film coefficients and admittance.

9) The specified times for printing data are tabulated.

10) The final portion of this type of output is a listing of any volume weighted internal on area weighted surface averages.

A.2.3 Calculation Output

The remainder of the printed output contains quantities calculated by ESATA. For each time increment, the following is printed:

1) The number of iterations required for program convergence.

2) CRIC - The value for the temperature convergence criteria needed in order to satisfy the heat flow convergence criteria (CRIT) input on Card 4.

3) Time increment.

4) Time of time step.

5) Cycle time for time step.

For each specified printout time and for the final time, the following data are output:

1) The problem title (as defined on Card 2 of the input data).

2) The printout time.

3) A matrix identifying the temperature of each internal node.

4) A matrix identifying surface node temperatures, film coefficients and surface heat flux.

5) A matrix identifying temperatures of each boundary node.

6) The total heat generated in the system, the heat transferred from the surfaces and the heat stored in the system.

7) A matrix identifying the heat generated in each node due to radioactive waste material.

8) A matrix identifying the heat generated in each node due to hydride dissociation.

9) A matrix identifying the material number (IMAT) and for each node fraction of the node (XMEL) that has melted.

10) A matrix identifying the fraction of dissociation for each hydride node.

11) The output of the maximum containment vessel temperature, the internal pressure, the stress level, and the fraction of the creep rupture life of the containment vessel consumed completes the data printout.

12) Should the number of iterations to achieve convergence exceed that specific or input data Card 4 (ERFC), then a statement is printed indicating an "Anomalous Problem" is printed.

13) Identification of the heat transfer rates from the waste container.

14) After the final output, a statement indicating "This problem completed" is printed.

APPENDIX B

PROPERTY DATA SUBROUTINES

B. 1 PROPERTY DATA USAGE

Property data used for the thermal transient calculations include thermal conductivity, specific heat, density and heat of fusion. The VARK subroutine is used to define the thermal conductivity for each node and calculates the thermal conductance between each node in the model. Thermal conductivity data is stored in the PROTK subroutine for materials 1-20. Data is read in for materials 21-40 for ESATA and normal TAP-A usage. Effective thermal conductivities are calculated in VARK for ESATA usage of materials 41-49.

The POWER subroutine is used to calculate the capacitance of each node. Specific heat data for materials 1-20 are stored in the PROCP subroutine and densities for materials 1-20 are stored in the DATA block. For materials 21-40, specific heat and density are read in. Effective specific heats and densities are calculated in CPCAL for materials 41-49. Heat of fusion data is provided for materials 1-20 in the DATA blocks and can be read in for materials 21-40. The TMPCAL subroutine used the heat of fusion data for materials 1-40 to consider the melting of any component plus the fuel (material 49).

The properties and equations for the calculation of effective properties for the various materials are documented below:

B. 1. 1 Thermal Conductivities for Materials 1-20

Material Number	Material	Temperature, ^{o}R	Thermal Conductivity Btu/(sec in ^{o}R)
1	Actinides	720	.001792
		1440	.001585
		2160	.001417
		2880	.001288
		3600	.001204
		4320	.001148
		5040	.001120

Material Number	Material	Temperature, °R	Thermal Conductivity Btu/(sec in °R)
2	Uranium Oxide	855	$.700 \times 10^{-4}$
		1391	$.527 \times 10^{-4}$
		1640	$.465 \times 10^{-4}$
		2291	$.364 \times 10^{-4}$
		2474	$.318 \times 10^{-4}$
		3019	$.265 \times 10^{-4}$
		3494	$.258 \times 10^{-4}$
3	SS-316	540	1.34×10^{-4}
		720	1.57×10^{-4}
		1080	2.07×10^{-4}
		1440	2.55×10^{-4}
		1800	3.05×10^{-4}
		2160	3.70×10^{-4}
4	LiH	720	1.37×10^{-4}
		900	1.04×10^{-4}
		1080	0.84×10^{-4}
		1260	0.73×10^{-4}
		1440	0.67×10^{-4}
5	Tungsten	540	0.00269
		720	0.0021
		1440	0.00174
		2160	0.00154
		2880	0.00143

Material Number	Material	Temperature, °R	Thermal Conductivity Btu/(sec in °R)
	Tungsten (Continued)	3600	0.00132
		4320	0.00129
		5580	0.00120
6	SS-316	540	1.34×10^{-4}
		720	1.57×10^{-4}
		1080	2.07×10^{-4}
		1440	2.55×10^{-4}
		1800	3.05×10^{-4}
		2160	3.70×10^{-4}
7	Water	492	7.38×10^{-6}
		564	8.4×10^{-6}
		636	8.94×10^{-6}
		708	9.17×10^{-6}
		816	9.03×10^{-6}
		888	8.73×10^{-6}
		960	8.17×10^{-6}
		1032	7.22×10^{-6}
		1460	6.94×10^{-6}
8	Mink 2020	660	3.28×10^{-7}
		1060	4.05×10^{-7}
		1260	4.5×10^{-7}
		1460	5.02×10^{-7}
		1660	5.54×10^{-7}
		1860	6.18×10^{-7}
		2060	6.85×10^{-7}

Material Number	Material	Temperature, ^{o}R	Thermal Conductivity Btu/(sec in ^{o}R)
9	Lithium	800	0.579×10^{-3}
		1000	0.635×10^{-3}
		1200	0.685×10^{-3}
		1400	0.73×10^{-3}
		1600	0.768×10^{-3}
		1800	0.80×10^{-3}
		2000	0.826×10^{-3}
		2200	0.846×10^{-3}
10	Coastal Plains Soil	671	3.75×10^{-6}
		851	4.01×10^{-6}
		1211	4.55×10^{-6}
		1571	5.35×10^{-6}
		1931	6.29×10^{-6}
		2291	7.49×10^{-6}
		2651	10.0×10^{-6}
		2831	12.84×10^{-6}
		3011	18.5×10^{-6}
		3191	29.4×10^{-6}
		3371	49.5×10^{-6}
		3461	64.2×10^{-6}
11	Granite Detrital Soil	671	0.99×10^{-5}
		1571	0.99×10^{-5}
		1931	1.0×10^{-5}
		2291	1.097×10^{-5}
		2651	1.40×10^{-5}
		2831	1.93×10^{-5}
		3011	3.35×10^{-5}
		3191	6.96×10^{-5}
		3371	20.1×10^{-5}

Material Number	Material	Temperature, $^{\circ}R$	Thermal Conductivity Btu/(sec in $^{\circ}R$)
12	Laterite Soil	671	0.174×10^{-5}
		1931	0.174×10^{-5}
		2291	0.401×10^{-5}
		2651	1.14×10^{-5}
		2831	1.85×10^{-5}
		3011	2.94×10^{-5}
		3191	4.41×10^{-5}
		3371	6.55×10^{-5}
		3461	7.89×10^{-5}
		3551	20.1×10^{-5}
13	Water	492	7.38×10^{-6}
		464	8.4×10^{-6}
		636	8.94×10^{-6}
		708	9.17×10^{-6}
		816	9.03×10^{-6}
		888	8.73×10^{-6}
		960	8.17×10^{-6}
		1032	7.22×10^{-6}
		1462	6.94×10^{-6}
14	Copper	720	$.91 \times 10^{-3}$
		1080	$.722 \times 10^{-3}$
		1170	$.733 \times 10^{-3}$
		1260	$.744 \times 10^{-3}$
		1440	$.76 \times 10^{-3}$
		1800	$.821 \times 10^{-3}$
		2160	$.888 \times 10^{-3}$
		2520	$.966 \times 10^{-3}$
		2700	1.01×10^{-3}

B. 1. 2 Specific Heat for Materials 1-20

Material Number	Material	Temperature, °R	Specific Heat Btu/lb °R
1	Actinides	535	.06
		660	.063
		960	.07
		2460	.08
2	Aluminum	560	.2
		760	.2
		960	.2
		1160	.2
3	SS-316	540	0. 140
		900	0. 142
		1080	0. 149
		1440	0. 162
		1880	0. 175
		2169	0. 110
		2520	0. 148
		2880	0. 170
		2949	0. 170
		2950	2. 5
		3000	2. 5
		3001	0. 17

Material Number	Material	Temperature, °R	Specific Heat Btu/lb °R
4	Lithium Hydride	540	0.84
		720	1.04
		900	1.19
		1080	1.33
		1260	1.48
		1440	1.62
		1620	1.76
		1699	1.76
		1700	31.6
		1750	31.6
		1751	1.76
5	Tungsten	540	0.0315
		720	0.032
		1440	0.034
		2160	0.036
		2880	0.0375
		3600	0.039
		4320	0.041
		5580	0.044
		6549	0.044
		6550	1.49
		6600	1.49
		6601	0.044

Material Number	Material	Temperature, °R	Specific Heat Btu/lb °R
6	SS-416	540	0.11
		720	0.115
		1080	0.12
		1440	0.13
		1800	0.15
		2160	0.18
		2759	0.18
		2760	2.66
		2810	2.66
		2811	0.18
7	Water	492	1.0
		1165	1.0
		1165.1	0.5
		2000	0.5
8	Mink 2020	1260	0.246
		2460	0.279
		3259	0.279
		3260	0.279
		3310	0.279
		3311	0.279
9	Lithium	500	0.996
		1500	0.996
		3000	0.996
10	Coastal Plains Soil	671	0.2
		2290	0.2
		3099	0.2
		3100	0.2
		3150	0.2
		3151	0.2

Material Number	Material	Temperature, °R	Specific Heat Btu/lb °R
11	Granite Detrital Soil	670	
			0.2
		2929	
			0.2
		2930	
			0.2
		2980	
			0.2
		2981	
			0.2
12	Laterite Soil	670	
			0.2
		3099	
			0.2
		3100	
			0.2
		3150	
			0.2
		3151	
			0.2
13	Water	492	
			1.0
		1165	
			1.0
		1165.1	
			0.5
		2000	
			0.5
14	Copper	540	
			0.092
		900	
			0.092
		1620	
			0.092
		3160	
			0.092

B. 1.3 Density and Heat of Fusion for Materials 1-20

Material Number	Material	Density lb/in^3	Melting Point Temperature, ^oR	Heat of Fusion lb/in^3
1	Actinides	.355	5444	64.5
2	Aluminum	.098	1660	170.
3	SS-316	.297	2760	127.5
4	Lithium Hydride	.0245	1720	1580.
5	Tungsten	.697	6550	74.5
6	Graphite	.093	7060	8.
7	Teflon	.079	1070	12.5
8	Mink 2020	.016	3260	14.
9	Lithium	.017	-	49.8
10	Coastal Plains	.0484	3390	10.
11	Granite Detrital	.0694	2760	10.
12	Laterite	.0539	3950	10.
13	Water	.079	-	-
14	Marinite	.0376	-	18.5

B. 1.4 Effective Thermal Conductivity, Specific Heat, Density and Heat of Fusion

Material Number	Description and Defining Equations and Assemptions
41	High Thermal Conductivity Axially in Cylinder Nodes and Circumferentially in Spherical Nodes

If IDEMK = 1 K = 1.0 Btu/sec inch ^oR

If IDEMK = 0 K = 0.000001 Btu/sec inch ^oR

Cp = 1.242 Btu/lb ^oR

ρ = 0.000001 lb/in^3

Material Number	Description and Defining Equations and Assemptions
41	High Thermal Conductivity Radially in Cylindrical and Spherical Nodes If IDEMK = 0 K = 1.0 Btu/sec inch ^{o}R If IDEMK = 1 K = 0.000001 Btu/sec inch ^{o}R Cp = 1.242 Btu/lb ^{o}R ρ = 0.000001 lb/in^3
42	High Thermal Conductivity in Both Directions K = 1.0 Btu/sec in ^{o}R Cp = 1.242 Btu/lb ^{o}R ρ = 0.000001 lb/in^3
43	High Thermal Conductivity in Both Directions K = 1.0 Btu/sec in ^{o}R Cp = 1.242 Btu/lb ^{o}R ρ = 0.000001 lb/in^3
44	Vessel to Soil Interface If IDEMK = 0.0 HT = 0.00193 Btu/sec in^2 ^{o}R IDEMK = 1.0 HT = 0.00000193 $K = HT\ \delta_{layer}$ $Cp = Cp_{coastal\ plains}$ $\rho = \rho_{coastal\ plains}$

Material Number	Description and Defining Equations and Assemptions
45	Vessel to Air Interface

T_1 = adjacent vessel node temperature

T_2 = *ambient temperature*

$\epsilon = 0.8$

$F = 1.0$

$H_r = \epsilon\, F\, 3.33 \times 10^{-15} (T_1{}^3 + T_1{}^2\, T_2 + T_1\, T_2{}^2 + T_2{}^3)$ Btu/sec in^2 ^oR

$Hc = 0.3667 \times 10^{-6}\ (T_1 - T_2)^{0.333}$ Btu/sec in^2 ^oR

$H_T = H_c + H_r$

$K = H_T\ \delta_{layer}$

where δ_{layer} *is the layer thickness*

$Cp = 0.24$ Btu/lb ^oR

$\rho = 0.02297/T_{air}$ lb/in^3

46	Air Nodes

$K = 1.0$

If connection is between air and soil

$HT = 0.424 \times 10^{-6}\ (T_{air} - T_{soil})^{0.333}$

where δ_{layer} *is distance from surface to air node center*

$Cp = 0.24$ Btu/lb ^oR

$\rho = 0.02297/T_{air}$ lb/in^3

Material Number	Description and Defining Equations and Assumptions
47	Vessel to Water Interface

$HT = 1.929 \times 10^{-4}$ Btu/sec in ^{o}R

$K = HT \; \delta_{layer}$

$Cp = 1.0$ Btu/lb ^{o}R

$\rho = \rho_{H_2O}$

48 *Dissociated LiH*

$K = K_{Li}$

$Cp = Cp_{LiH}$

$\rho = \rho_{LiH}$

49 Homogeneous Wast Product Composite

$$\rho = \frac{W_{Al} + W_{fuel} + W_{Cu} + W_{LiH}}{Vol_c}$$

$$Cp = \frac{W_{Al}\, Cp_{Al} + W_{fuel}\, Cp_{fuel} + W_{Cu}\, Cp_{Cu} + W_{LiH}\, Cp_{LiH}}{W_{Al} + W_{fuel} + W_{Cu} + W_{LiH}}$$

$K = 17$ Btu/(hr-ft-^{o}R)

APPENDIX C

DESCRIPTION OF ESATA PROGRAM VARIABLES

DESCRIPTION OF ESATA - II PROGRAM VARIABLES

NOTE: For those matrices having fixed dimensions in the program, the size is indicated in the following table:

FORTRAN SYMBOL	ENGINEERING SYMBOL	DESCRIPTION	UNITS
CAP (I)	C	Heat Capacity of Node I	Btu/^{o}R
QINTO (I)	Q_f	Total Heating Rate in Node I due to Fission Products	Btu/sec.
T (I)	T_{τ}	Temperature of Node I	^{o}R
TEMRAT (I)	$T_{\tau-1}$	Temperature of Node I at Previous Time Step	^{o}R
VOL (I)	V	Volume of Node I	In.^{3}
QINTI (I)	Qr	Total Heating Rate in Node I Due to Metal/Water Reactions	Btu/sec.
SUMM (I)	--	Product of CAP (I) and T (I)	Btu
TNEW (I)	--	Intermediate Temperature for Node I Computed During Iteration Process	^{o}R
Y (I, J)	Y	Admittance Between Node I and Node Defined By IJ (I, J) for Connection J	Btu/sec-^{o}R
IJ (I, J)	--	Matrix Identifying Node Connected to Node I by Connection J	Dimensionless
OLDCON (I, J)	--	One Half the Thickness of Node I Divided by the Surface Area Between Node I and Node J	In^{-1}
CC (I, J)		Matrix Identifying Surface to Boundary Node Heat Transfer Mechanism	Dimensionless
H (I, J)	H	Heat Transfer Coefficient Between Surface Node I and Boundary Node IJS (I, J)	Btu/sec-In^{2}-^{o}R
SAREA (I)	A	Surface Area of Node I	In^{2}
ST (I)	T_s	Surface Temperature of Node I	^{o}R
YS (I)	Y_s	Admittance Between Node I and Boundary Surface of Node I	Btu/sec-^{o}R
IJS (I, J)	--	Matrix Identifying Boundary Node Connected to Surface Node I by Connection J	Dimensionless
BT (I)	T_B	Boundary Temperature of Node I	^{o}R
IB (I)	--	Heat Transfer Coefficient Table Number	Dimensionless
TB (I, J)	$T_B(\tau)$	Boundary Temperature of Node I if Time Dependent	^{o}R
IT (I, J)	τ	Time Corresponding to TB (I, J)	Seconds
INNE (I)	--	Index Identifying Entrance Point in Boundary Temperature/Time Table	Dimensionless
INNO (I)	--	Maximum Number of Entries in Each Boundary Temperature/Time Table	Dimensionless
TQ (I)	τ	Maximum Number of Entries in Each Boundary Temperature/Time Table	Dimensionless
QQ (I)	--	Power Factor Corresponding to QINTO (I)	Dimensionless

FORTRAN SYMBOL	ENGINEERING SYMBOL	DESCRIPTION	UNITS
QN (I)	--	Power Factor Corresponding to QINTI (I)	Dimensionless
PRNT (I)	--	Time Point at Which Data is to be Printed	Seconds
TAT (I)	τ, T	Time or Temperature Difference Variable for Film Coefficient Tables	Seconds, ^oR
HAH (I)	$H(\tau)$, H(T)	Time or Temperature Difference Dependent Film Coefficient	Btu/sec-in^2-^oR
IP (I)	--	Number of Entries in Each Film Coefficient Table	Dimensionless
INO (I)	--	Index Identifying Entrance Point in Film Coefficient Tables	Dimensionless
ININ (I)	--	Starting Node Index for Weighted Averages	Dimensionless
INIM (I)	--	Ending Node Index for Weighted Averages	Dimensionless
IMAT (I)	--	Matrix Identifying Material Number for Node I	Dimensionless
ICC (I)	--	Matrix Identifying Connector Type	Dimensionless
IJT (I, J)	--	Connector Node Index Identifier for Secondary Node	Dimensionless
AOL (I, J)	--	Length/Area Ratio for Primary Node	In^{-1}
AOLJ (I, J)	--	Length/Area Ratio for Secondary Node	In^{-1}
IDEMK (I, J)	--	Matrix Identifying Nodes Having Orthotropic Conductivity	Dimensionless
IDEMKJ (I, J)	--	Matrix Identifying Nodes Having Orthotropic Conductivity	Dimensionless
MAXINT	--	Maximum Number of Internal Nodes	Dimensionless
MAXSUR	--	Maximum Number of Surface Nodes	Dimensionless
MAXBND	--	Maximum Number of Boundary Nodes	Dimensionless
MAXCON	--	Maximum Number of Internal Connectors per Node	Dimensionless
MAXRAD	--	Maximum Number of Surface/Boundary Node Connectors	Dimensionless
MAXTAB	--	Maximum Number of Boundary Temperature Tables	Dimensionless
MTABEN	--	Maximum Number of Boundary Table Entries	Dimensionless
MAXQQ	--	Maximum Number of Power Table Entries	Dimensionless
MAXPRT	--	Maximum Number of Printout Times	Dimensionless
MAXFIL	--	Maximum Number of Film Coefficient Tables	Dimensionless
MFILEN	--	Maximum Number of Film Coefficient Table Entries	Dimensionless
IMAXAV	--	Maximum Number of Averages	Dimensionless
MAXTYP	--	Maximum Number of Connector Types	Dimensionless

FORTRAN SYMBOL	ENGINEERING SYMBOL	DESCRIPTION	UNITS
LSI to L540	--	Computer Storage Starting Locations for the Previously Defined Matrixes	Dimensionless
RO (20)	R_I	OuterRadius for Each Radial Layer of Spherical Nodes	In
LAYMAT (20)	--	Material Number for Each Radial Layer of Spherical Nodes	Dimensionless
TEMLAY (20)	T_ℓ	Initial Temperature for Each Layer of Spherical Nodes	^{o}R
THC (40)	ΔX	Radial Thickness for Layer of Spherical Nodes and Vertical Thickness for Layers of Cylindrical Nodes in Base	In
VOLDEN (60)	ρ	Density Matrix for Materials	Lb/In^3
WEIGHT (4)	W	Weight of 4 Fuel Constituents	Lbs
TMP (60)	T_{mp}	Melting Point Temperature Matrix for Materials	^{o}R
HFUS (60)	H_{fg}	Heat of Fusion	Btu/lb-^{o}F
ISTI (6)	--	Matrix Identifying Top Node in Each of 6 Rows of Nodes Inside Spherical Layers for Deep Burial Model	Dimensionless
CAPMAT (40)	Cp	Specific Heat Matrix for Materials Having a Constant Value	Btu/Lb-^{o}R
VOLCON (40)	K	Thermal Conductivity Matrix for Materials Having a Constant Value	Btu/sec. - In ^{o}R
TET (100)	T	Temperature Parameter for Heat Capacity and Thermal Conductivity Temperature Dependent Tables	^{o}R
VCAP (100)	Cp (T)	Temperature Dependent Specific Heat	Btu/Lb - ^{o}R
VCON (100)	K (T)	Temperature Dependent Thermal Conductivity	Btu/sec. - in ^{o}R
JL (10)	--	Number of Material Properties for Each Property Table	Dimensionless
ID (14)	--	Matrix for Reading the Case Title	Dimensionless
Z (10)	--	"Scratch" Matrix Used in Different Parts of the Computation Sequence	Variable
IT (10)	--	Printout Index for Printing Admittances	Dimensionless
VOLCOT (40)	K	Thermal Conductivity for Those Materials Having Orthotropic Properties	Btu/sec.-In ^{o}R
AE	--	"Scratch" Parameter used in Several Different Computations	Variable
AO	--	"Scratch" Parameter used in Several Different Computations	Variable
CRITIM	--	Dummy Variable	Dimensionless
CRIT	--	Heat Flow Convergence Criteria	Dimensionless

FORTRAN SYMBOL	ENGINEERING SYMBOL	DESCRIPTION	UNITS
DELTAT	Δ	Time Increment	Seconds
OLDCAP	--	Dummy Variable	Dimensionless
QINT	Qt	Total Heat Generation Rate	Btu/sec.
TAVG	Tavg	Average Temperature	^oF
TIMEO		Initial Time	Seconds
TIME		Time	Seconds
TIMFIN		Final Time	Seconds
TYM	--	Dummy Variable	Dimensionless
IBMAX	--	Index for Maximum Number of Boundary Nodes	Dimensionless
ICON	--	Dummy Variable	Dimensionless
ICOV	--	Dummy Variable	Dimensionless
IMAX	--	Index for Maximum Number of Internal Nodes	Dimensionless
I, J, K, L		Indicies	Dimensionless
ISMAX	--	Index for Maximum Number of Surface Nodes	Dimensionless
ISTOP		Automatically Stops Program if Solution is not Converged after Predefined Number of Iterations	Dimensionless
IERROR		Automatically Stops Program if Input Error is Detected	Dimensionless
ISUN		"Scratch" Parameter Used in Different Computations	Variable
LIBQ	--	Maximum Number of Power Factor Entries	Dimensionless
LIBT		Dummy Variable	Dimensionless
LIBTT		Dummy Variable	Dimensionless
MATA, MATB		Material Number Index	Dimensionless
MET		Material Number Index	Dimensionless
MAXBAD		Dummy Variable	Dimensionless
MAXMAT		Maximum Material Number Available for Input	Dimensionless
MAXS2		Dummy Variable	Dimensionless
MAXS		MAXRAD Plus One	Dimensionless
NB		Boundary Node Base	Dimensionless
LIBQT		Index Identifying Entrance Point in Power Factor Table	Dimensionless

FORTRAN SYMBOL	ENGINEERING SYMBOL	DESCRIPTION	UNITS
NISB	--	NB + MAXBND	Dimensionless
NIS	--	NS + MAXSUR	Dimensionless
NP	--	Counter for the Number of Times Data is Printed	Dimensionless
NS	--	Surface Node Base	Dimensionless
NUMPRT	--	Total Number of Printout Times	Dimensionless
NACCL	--	Number of Iterations Prior to Temperature Extrapolation	Dimensionless
IPT	--	Problem Type Indicator (Transient or Steady State)	Dimensionless
QMULT	--	Power Factor Corresponding to QINTO (I)	Dimensionless
QMULT2	--	Power Factor Corresponding to QINTI (I)	Dimensionless
NMAX	--	Maximum Number of Iterations	Dimensionless
IMAXAV	--	Maximum Number of Averages	Dimensionless
IMAAV	--	Number of Averages Requested	Dimensionless
VAR	--	Problem Type	Dimensionless
IAMCOR (80)	--	Array Defining those Nodes Representing the Fueled Core	Dimensionless
XMEL (300)	--	Fraction of Melting for Each Node	Dimensionless
TOLD (300)	T'	Temperature of Each Node Corresponding to Previous Time Step	^oR
SLAY (17)	S	Layer Thickness for Defining Effective Conductivities for Materials	In.
VHD (300)	V_{hyd}	Void Volumes Representing Hydride Nodes	$In.^3$
NH2T (300)	N_{H2}	Number of Hydrogen Molecules in Each Node of Hydride Material	Dimensionless
XDIS (300)	X_{DIS}	Fraction of Dissociation for Each Hydride Node	Dimensionless
IHD (300)	--	Array Defining Nodes Representing Hydride Material	Dimensionless
ISATA	--	Parameter Identifying Choice of Normal TAP-A, Normal ESATA, or ESATA Restart Option	Dimensionless
IMODEL	--	Basic Heat Transfer Model (Deformed, Undeformed)	Dimensionless
IBURY	--	Degree of Soil Burial	Dimensionless
PTOT	P	Internal Pressure	$Lbs/In.^2$
TCOR	T_c	Fuel Temperature	^oR
TAMB	Ta	Ambient Temperature	^oR
TSOIL	Ts	Soil Temperature	^oR
VOLC	Vc	Volume of Nodes Representing Fuel	$In.^3$

FORTRAN SYMBOL	ENGINEERING SYMBOL	DESCRIPTION	UNITS
IHTI-IHTA	--	Intermediate Parameters in Hydride Calculation	Dimensionless
ISHMAX	--	Maximum Index for Shield Nodes	Dimensionless
VVOID	--	Total Void Volume in System	$In.^3$
MLIH2	$M_{H2, LiH}$	Weight of Gaseous Hydrogen Released for LiH Dissociation	Lbs.
NHD	N_{H2}	Number of Moles of Gaseous Hydrogen Released from Hydride Dissociation	Dimensionless
TNH2L	$NT_{H2, LiH}$	Total Number of Hydrogen Moles in LiH	Dimensionless
VOLIH	V_{LiH}	Total Volume of LiH	$In.^3$
WTLIH	W_{LiH}	Total Weight of LiH	Lbs.
TNLIH	NT_{LiH}	Total Number of LiH Moles	Dimensionless
COMPAC	--	Fraction of Containment Vessel Compaction	Dimensionless
NRCV	--	Layer Number Representing Outer Layer of Containment Vessel	Dimensionless
RCNTV	R_{CV}	Inner Radius of Containment Vessel	Inches
DCNTV	S_{CV}	Thickness of Containment Vessel	Inches
AOXRAT	$(A/L)_{CV}$	Area to Thickness Ratio for Containment Vessel	Inches
NCVLAY	--	Number of Layers Representing Containment Vessel	Dimensionless
NCOR	--	Number of Nodes Representing Fueled Core Nodes	Dimensionless
DELRST	--	Cp Time Increment for Storing Common Block Date on Restart Tape	Dimensionless
INTMAT	--	*Interface Material* Number	
DCORE	--	*Time Step - Intermediate Value for Acceleration Technique*	Sec.

Astronuclear Laboratory

DISTRIBUTION LIST

NUCLEAR RADIOACTIVE WASTE DISPOSAL IN SPACE STUDY GROUP

10 Mr. Herbert Schaefer
Code MTE
National Aeronautics and
Space Administration
Washington, D.C. 20546

1 Mr. Thomas Kerr
Code RY
National Aeronautics and
Space Administration
Washington, D.C. 20546

1 Mr. Joseph McGolrick
Code SV
National Aeronautics and
Space Administration
Washington, D.C. 20546

1 Dr. Hans Mark, Director
NASA-Ames Research Center
Moffett Field, CA 94035

1 Mr. John MacKay
Code MS
NASA-Ames Research Center
Moffett Field, CA 94035

1 Mr. John Vorreiter
Code STM
NASA-Ames Research Center
Moffett Field, CA 94035

1 Mr. Richard Wood
Code MO
NASA-Ames Research Center
Moffett Field, CA 94035

1 Mr. Thaddeus J. Dobry
Code SNS
AEC-NASA Space Nuclear
Systems Office
Washington, D.C. 20545

10 Mr. Robert W. Ramsey, Jr.
Code WMT
AEC
Washington, D.C. 20545

1 Mr. Charles Tynan/MS-418
NASA-Langley Research Center
Hampton, VA 23365

Mr. James A. Sisler
Code WMT
AEC
Washington, D.C. 20545

1 Mr. Frank X. Gavigan
Code SNS
AEC-NASA Space Nuclear
Systems Office
Washington, D.C. 20545

1 Mr. Victor R. Bond
Code FM-8
NASA-Manned Spacecraft Center
Houston, TX 77058

1 Mr. Gus Babb
Code FM-8
NASA-Manned Spacecraft Center
Houston, TX 77058

10 Dr. Kirk Drumheller
Battelle Northwest
Battelle Memorial Institute
Richland, WA 99352

1 Mr. Nat Loenig
Code IS-MED
NASA-Kennedy Space Center
Kennedy Space Center, FL 32899

1 Dr. John Russell
Gulf General Atomic
LaJolla, CA 92112

10 NASA Scientific & Technical Info.
Facility
Attention: Acquisition Branch
P. O. Box 33
College Park, MD 20740

DISTRIBUTION LIST (Continued)

NUCLEAR RADIOACTIVE WASTE DISPOSAL IN SPACE STUDY GROUP

	NASA-Lewis	MS
1	Frank Rom	500-201
1	Pat Finnegan	500-201
1	Millard Wohl	500-201
10	Dick Puthoff	500-201
1	Bob Thompson	500-318
1	Art Zimmerman	500-318
1	Bob Lubick	500-318
1	Ruth Weltmann	6-2
1	L. Schopen	500-206
1	Norm Musial	500-113
2	Lewis Library	60-3
1	Report Control	5-5